ARL-TR-10434 ● SEP 2026

Energetic Properties Prediction Interface (EPPI) Validation for Carbon, Hydrogen, Nitrogen, Oxygen, and Fluorine (CHNOF) Materials

by William Mattson, Joshua Lansford, and Brian Barnes

NOTICES

Disclaimers

The findings in this report are not to be construed as an official Department of the Army position unless so designated by other authorized documents.

Citation of manufacturer's or trade names does not constitute an official endorsement or approval of the use thereof.

Destroy this report when it is no longer needed. Do not return it to the originator.

ARL-TR-10434 ● SEP 2026

Energetic Properties Prediction Interface (EPPI) Validation for Carbon, Hydrogen, Nitrogen, Oxygen, and Fluorine (CHNOF) Materials

William Mattson, Joshua Lansford, and Brian Barnes
DEVCOM Army Research Laboratory

REPORT DOCUMENTATION PAGE

1. REPORT DATE	2. REPORT TYPE	3. DATES COVERED	
		START DATE	END DATE
September 2026	Technical Report	10/1/2025	9/30/26

4. TITLE AND SUBTITLE
Energetic Properties Prediction Interface (EPPI) Validation for Carbon, Hydrogen, Nitrogen, Oxygen, and Fluorine (CHNOF) Materials

5a. CONTRACT NUMBER	5b. GRANT NUMBER	5c. PROGRAM ELEMENT NUMBER
5d. PROJECT NUMBER	5e. TASK NUMBER	5f. WORK UNIT NUMBER

6. AUTHOR(S)
William Mattson, Joshua Lansford, and Brian Barnes

7. PERFORMING ORGANIZATION NAME(S) AND ADDRESS(ES)	8. PERFORMING ORGANIZATION REPORT NUMBER
DEVCOM Army Research Laboratory ATTN: FCDD-RLA-WA Aberdeen Proving Ground, MD 21005	ARL-TR-10434

9. SPONSORING/MONITORING AGENCY NAME(S) AND ADDRESS(ES)	10. SPONSOR/MONITOR'S ACRONYM(S)	11. SPONSOR/MONITOR'S REPORT NUMBER(S)

12. DISTRIBUTION/AVAILABILITY STATEMENT
DISTRIBUTION STATEMENT A. Approved for public release: distribution unlimited.

13. SUPPLEMENTARY NOTES
ORCIDs: William Mattson, 0000-0002-3922-1279; Joshua Lansford, 0000-0001-8245-3190

14. ABSTRACT
Energetic materials have a number of important properties affecting safety, manufacturability, and performance. Physics-based calculations of these properties range from computationally expensive to infeasible. Thermochemical codes can predict some of these properties, given quantities such as the density and heat of formation, but can be unreliable. Other properties can require difficult and expensive first-principles calculations. ML methods have shown promise for predicting many of the relevant properties for energetic materials simply from a 2D description of the molecules structure. We evaluate the performance of the Energetic Properties Prediction Interface (EPPI), a software suite of ML models packaged as a GUI with all dependencies included. We have gathered a dataset of nearly 300,000 molecules containing carbon, hydrogen, nitrogen, oxygen, and fluorine with at least one of the nine relevant experimental properties. While the models within EPPI were trained across a large set of materials, they were not specifically trained for materials containing fluorine. However, we find good results for many of the properties of fluorine-containing materials; therefore, the models demonstrate strong potential for transferability with relatively small datasets for new classes of materials.

15. SUBJECT TERMS
Weapons Sciences, machine learning, verification and validation, energetic materials, fluorine, material properties

16. SECURITY CLASSIFICATION OF:			17. LIMITATION OF ABSTRACT	18. NUMBER OF PAGES
a. REPORT	b. ABSTRACT	C. THIS PAGE		
UNCLASSIFIED	UNCLASSIFIED	UNCLASSIFIED	UU	54

19a. NAME OF RESPONSIBLE PERSON	19b. PHONE NUMBER *(Include area code)*
William Mattson	(520) 691-5662

STANDARD FORM 298 (REV. 5/2020)
Prescribed by ANSI Std. Z39.18

Contents

List of Figures

Acknowledgments

The authors thank Robert Appleton (Energetics Technology Center) and Edward F.C. Byrd (ARL) for useful discussion and advice.

1. Introduction

The rapid prediction of material properties, particularly novel material properties, is of great interest (SMGICT 2021). This is especially true for energetic materials where measuring material properties can be costly and hazardous (Rae and Dickson 2021). Energetic materials, by design, rapidly release a significant portion of their stored energy; therefore, it is hazardous, time-consuming, and costly to produce, process, and test such materials. There are several properties that can determine if an energetic material is worth exploring experimentally; specifically, those affecting safety, manufacturability, and performance. However, these properties are computationally expensive, and in some cases impossible to predict from first principles (Yan and Zeman 2013), or even dramatically simplified physical models (Han et al. 2018; Sen et al. 2018). While thermochemical codes can predict some of these properties given quantities such as the density and Heat of Formation (HoF) (Fried and Souers 1994; Nieto-Draghi C et al. 2015), computing these two quantities from first principles, particularly the density, can be excessively time consuming. Calculating the density requires a knowledge of the melting and perhaps boiling point of the material, and, if it is known to be a solid, the crystalline symmetry is also required. Searching for an undetermined crystal structure of a material or performing simulations to determine the liquid density at ambient pressure, or even simulations to determine the melting point of a material, are research projects of their own. Other methods are therefore needed to rapidly determine the feasibility of an energetic material.

While there are a number of properties of interest for these materials, this work focuses on nine properties. The properties calculated are the 1) density, 2) HoFs, 3) detonation velocity, 4) detonation pressure, 5) impact sensitivity (H_{50}), 6) melting temperature, 7) boiling temperature, 8) decomposition temperature, and 9) vapor pressure. First, density is a key indicator of energetic material performance. Second, the HoF is indicative of how much energy is stored in a material and therefore how much energy can potentially be released by it. Next, the detonation velocity and pressure are measures of how fast a material can release energy and how much of that energy can be used for mechanical work. Fifth, impact sensitivity is also a measure of how safely a material can be stored. Herein the sensitivity as a function of the energy of impact is examined, for which the height of a drop weight where the material reacts 50% of the time is a common measure and termed the H_{50}. The melting, boiling, and decomposition temperatures, along with the vapor pressure, are used to determine how and whether a material can be melt cast, safely processed, along with how stable it will be during storage. For example, high vapor

pressure means that the material will likely be very volatile. Conversion between the two is possible if the mass of the impactor is known.

Some statistical methods have shown promise for predicting many of the relevant properties for energetic materials (Honda et al. 2019; Chithrananda et al. 2020; Winter et al. 2022; Heid et al. 2024). The Energetic Properties Prediction Interface (EPPI) (Lansford et al. 2022, 2023; Appleton et al. 2024, 2025a, 2025b, 2026; Lansford and Barnes 2025) uses an ensemble of message-passing neural networks (Gilmer et al. 2017) to predict properties from a 2D description of the molecules' structure, called a Simplified Molecular Input Line Entry System (SMILES) string (Weininger 1988).

We have gathered multiple datasets and searched through the literature to evaluate EPPI by generating a combined dataset of over 300,000 molecules containing carbon, hydrogen, nitrogen, oxygen (CHNO) and fluorine (CHNOF) with at least one of the nine aforementioned relevant properties. While the model was trained across a large set of materials, it was not specifically trained for materials containing fluorine. However, we found good results for many of the properties of fluorine-containing materials; therefore, the model demonstrates strong potential for transferability with relatively small datasets for new classes of materials.

In the following sections we will discuss EPPI, our methods of data collection, and how we culled that data to the most relevant subset that is presented in the results within Section 3. We then break up the results into subsections for each property to show validation and transferability of the model, and finish with concluding remarks.

2. Methods

2.1 EPPI

EPPI is a U.S. Army Combat Capabilities Development Command (DEVCOM) Army Research Laboratory (ARL)-developed code that uses a set of ML models to calculate the nine different properties relevant for the assessment of energetic materials and their expected standard errors in the mean (SEs). Results from each of the two different models are used for calculating the density, melting temperature, and the impact sensitivity (H_{50}). Two different models for density were developed: one with data from quantum mechanics (QM) and the other with experimental data. The additional models for melting temperature and impact sensitivity were developed by Robert Appleton and are labeled RA. EPPI can run either interactively on a single material at a time or in batch mode.

EPPI initially opens a command window that displays progress loading the Python environment and importing necessary Python module. Once all necessary dependencies are loaded, an EPPI GUI window pops up with a progress bar showing the individual models being loaded into memory. A view of the EPPI GUI with single molecule predictions for pentaerythritol tetranitrate (PETN) can be seen in Figure 1.

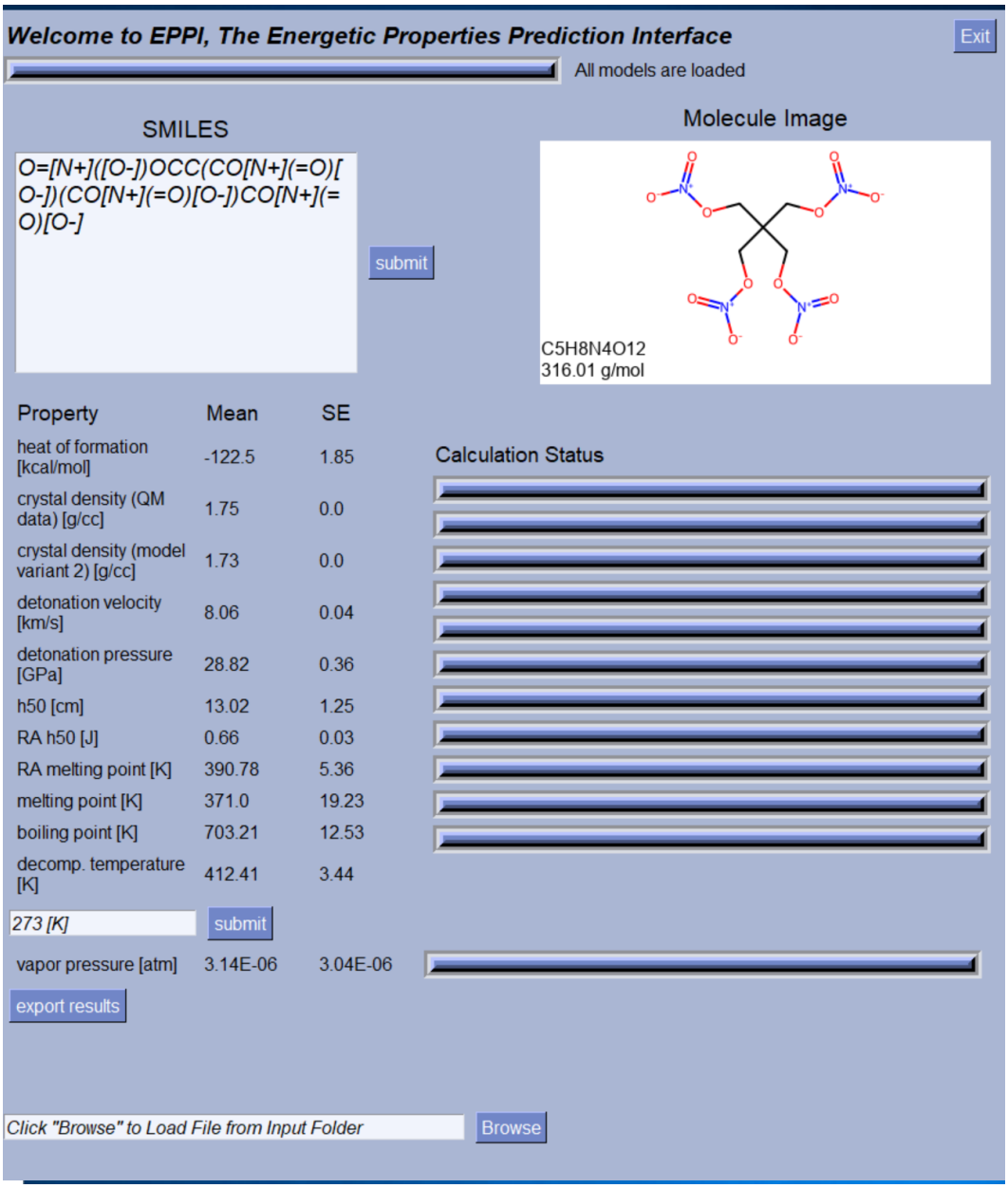

Figure 1. EPPI user interface with example SMILES string for PETN specifying vapor pressure temperature of 273 K. SMILES string is entered into the textbox at upper left; 2D molecular diagram at upper right; predicted properties at center left, followed by text box to enter the temperature at which to predict vapor pressure.

In single molecule mode, EPPI takes as input only an ASCII string that is a 2D representation of the molecular structure of the material in the form of a SMILES string and optionally the temperature for calculating the vapor pressure. If EPPI finds the SMILES string to be valid, it will replace the SMILES string in the text box with the canonicalized SMILES string (RDKit 2026). If not, it replaces the SMILES string with "Invalid SMILES." EPPI produces a 2D skeletal diagram of the molecule generated by RDKit for verification. As the calculation continues, a progress bar in the command window and GUI interface appear. Once the calculations have been completed, the mean values and SEs are shown, then the temperature for the desired vapor pressure can be entered in the text box towards the bottom left of the interface, and the submit button next to it can be used to start the vapor pressure calculation. The text box for the vapor pressure temperature will reset after each run, so the temperature must be reentered and the submit button pressed every time.

For a single material, EPPI produces a 2D visual representation of the molecular structure of the material for verification, and the image can be saved to a Portable Network Graphics file and the properties to a comma-separated value (CSV) file. This can be done by clicking the "export results" button towards the bottom-left corner. This will generate files in the "output_files" subdirectory of the directory from which EPPI is run. File names will have the following format: ChemicalFormula_Time.FileSuffix. Column titles are in the first row of the CSV file: SMILES, property, mean, and SE. Below are rows for each property calculated with the SMILES string, property name, predicted mean, and SE. The mean value is the ensemble average of multiple models trained on different subsets of data.

In batch mode, EPPI can take as input either a CSV or Excel spreadsheet with a single column with its first row labelled "smiles" and the subsequent rows being a SMILES string for a molecule. To do this, click the "browse" button at the bottom left of the GUI. This brings up a File dialog starting in the directory from which EPPI was run. Input files should be in the "input_files" subdirectory. The file can be selected by double-clicking it or selecting it and clicking "open." This begins the calculation. Progress for batch calculations is shown only in the command window. Batch runs are divided into sequential calculations where each individual model for a property calculates the value for every SMILES string before proceeding to the next property model, until all the models for a given property are completed and it moves to the next property. Progress for the completion of each model is shown in the command window. Upon completion of all the models, the run produces a CSV file located in the "output_files" subdirectory. The file name will have the prefix "ML_pred_" but is otherwise the same as the input file name. Its first row is column labels and each following row corresponds to the same

material specified by the SMILES string in the same row of the input file. For each of these material rows, the first column is the SMILES string, and then there are two columns for each property: the first for the mean value (the average of each individual model) and the second for the SE of the ensemble, which is labeled std instead of SE. Currently, the temperature for the vapor pressure calculation in batch mode is fixed at 400K, which is relevant to melt-cast explosives. The number entered into the temperature text box therefore has no effect during batch calculations. Example input and output files are included in the EPPI distribution in the "input_files" and "output_files" directories, respectively. EPPI is sensitive to malformed SMILES strings and will exit the calculation without saving the properties when it encounters one, so using large untested input files may be computationally wasteful.

2.2 Data Collection

The material property data used for comparison with EPPI in this report comes from several different sources. The first two sources are Appleton et al. (2025a) and Lansford et al. (2023). While they did not contain data for every material or property in the dataset, they contained many of the same materials and properties. Therefore, these two datasets were merged. The third source was the ChemPhys Space dataset (Muravyev et al. 2022), and it largely contained three properties relevant to energetic materials that were not in the initial dataset; namely the HoF and the detonation pressure and velocity. So, this dataset was kept separate, giving two unique datasets, a general material- and an energetic material-focused dataset. The final sources were a search of the literature, ThermoML (Frenkel et al. 2003), and other websites and datasets for data relevant to energetic materials and of interest to the DoD. Data from this search was used to augment the data in the two different datasets. The two different datasets are available in supplemental material that is available upon request, and each contains a column that specifies the original data source or sources. When the datasets were merged, the SMILES strings were converted to a canonical form with RDKit (2026). These canonical SMILES strings were then compared and, if they matched their values, were merged. For cases where there was more than one entry for a property, the values were averaged and the entries for the sources were combined into a list.

2.3 Data Filtration

The initial data collection effort included all materials that contained any of the following elements: carbon, hydrogen, oxygen, nitrogen (CHNO), or fluorine. This broad search was used to ensure that nothing relevant was missing; however, it did result in dataset that was too broad for our purposes. To avoid any issues with the

model that are not relevant to the current work, we filtered both datasets into two subsets. The first, which will be referred to as the CHNO dataset, contains materials that had at least two of, and only, the elements carbon, nitrogen, and oxygen, with possibly hydrogen. The second, which will be referred to as the CHNOF dataset, contains fluorine and at least one of, and only, the elements carbon, nitrogen, and oxygen, with hydrogen being optional. Outliers from both datasets (in terms of extreme values and significant disagreement with the EPPI results) were examined. Several of these values were from unorganized datasets and could not be verified, so these entries were removed and are in supplemental materials that are available upon request. Furthermore, some data was culled from the plots reported in this work for clarity of presentation; this data is also available upon request.

3. Results and Discussion

EPPI consistently underpredicted high values and overpredicted low values for the outliers that were removed from the dataset for clarity (mentioned above). This indicated a systemic bias in the model similar to a regression-to-the-mean type of behavior, and is not surprising for values significantly outside the range of data used in training the models. Below, we divide the results into sections by property, with separate sections for each model when more than one model group exists for a single property. The properties are listed in the order they occur in the EPPI GUI.

The following sections explore the predictive capability of EPPI by examining hexagonal bin plots comparing experimental measurements with EPPI's predicted values. The experimental values are displayed along the x-axis and predicted values along the y-axis. If there are hexagonal bins with more than one material in a bin, each bin will be colored by the number of materials in the bin, and a color bar will be displayed. Along with the hexagonal bin plot, the root mean square error (RMSE), mean absolute error (MAE), and Pearson correlation coefficient are given for each plot. These hexagonal bin plots along with tables of substructure distribution and the associated substructure RMSE, MAE and Pearson correlation coefficients and molecular weight and heavy atom number distributions for each property are given in Appendixes A and B.

3.1 HoF

The HoF data was taken from the energetic materials dataset, so the number of materials is relatively small. It can be seen in Figure 2 that this model (Appleton et al. 2025b) for CHNO materials contains good agreement between EPPI and experiment, with the outliers being more common at extreme values. For materials

containing fluorine, however, EPPI typically overpredicts the HoF—although it does somewhat better at predicting the ordering.

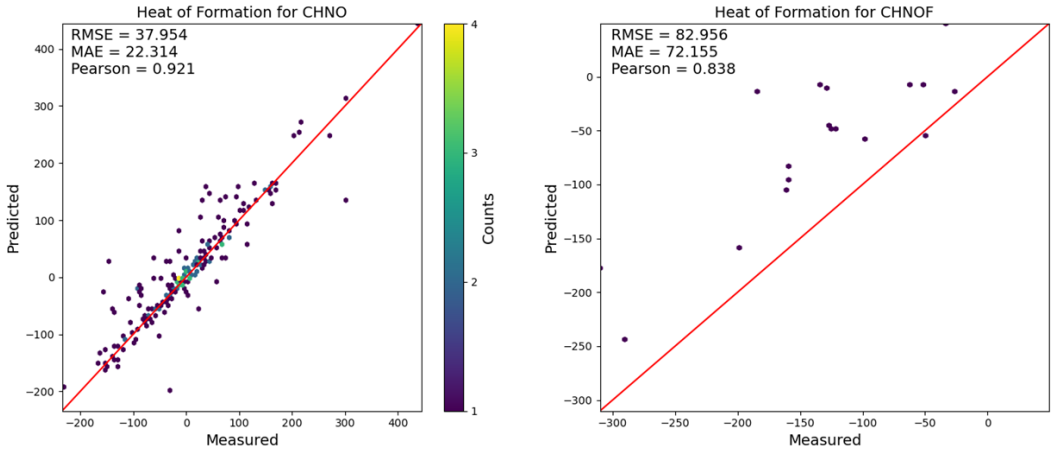

Figure 2. Comparison of measured and predicted HoF in kilocalories per mole for CHNO (left) and CHNOF (right).

3.2 Crystalline Density (Quantum Mechanical)

EPPI also calculates density with two different models. The first one was trained on density data from a set of methods using QM information to determine density in the software package EDAT (Byrd 2012). While the performance for CHNO materials is quite good, we see that for CHNOF materials this model systematically underpredicts for higher density materials. This type of deviation is not uncommon when trying to use a learned model beyond the range of its training data. Even with the underprediction at high densities, this model does quite well overall for CHNOF materials, as can be seen in the error metrics (Figure 3).

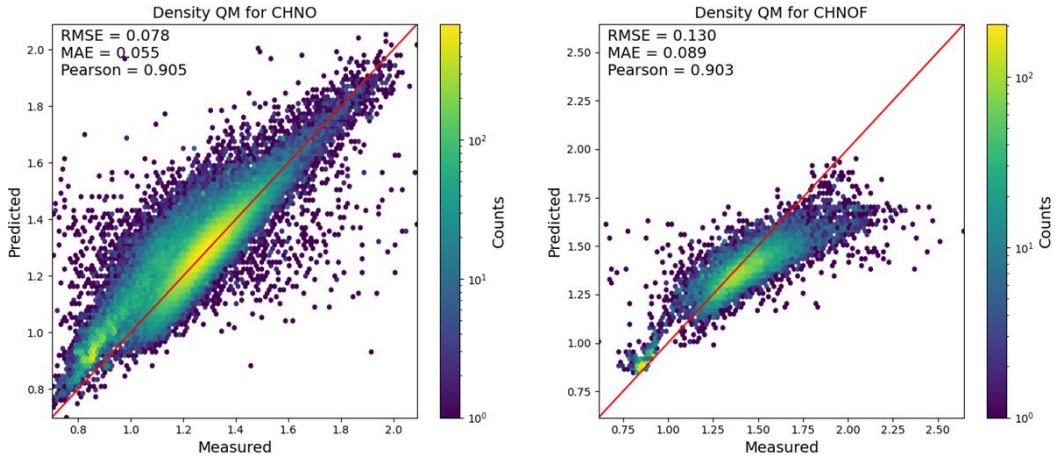

Figure 3. Comparison of measured and predicted crystalline density (QM) in grams per cubic centimeter for CHNO (left) and CHNOF (right).

3.3 Crystalline Density (Experimental)

This is a comparison of the dataset values with EPPI's predicted experimental density, which is labeled "model variant 2" in the interface. This model was trained on experimental data. This is the largest and most diverse property in the datasets, and EPPI does quite well at predicting the crystalline density for both CHNO and CHNOF. However, when faced with covalent solids or long chain polymers, EPPI underpredicts the density. Also, a close examination of Figure 4 shows two trends. The first starts out with good agreement at lower densities, getting worse as it tends towards moderate densities for both CHNO and CHNOF, where EPPI seems to overpredict. The second trend, going towards higher densities, where EPPI starts to slightly underpredict although the agreement is still very good, is seen more clearly for CHNOF materials. A substructure analysis of this trend may be in order, as the Pearson correlation coefficient for substructures runs as low as 0.48 for anthracene—markedly different from the drift noted above for the QM where the error metrics for the different substructures are relatively closely packed. It seems the QM method has better substructure representation, while the experimental method has better range and fluorine representation.

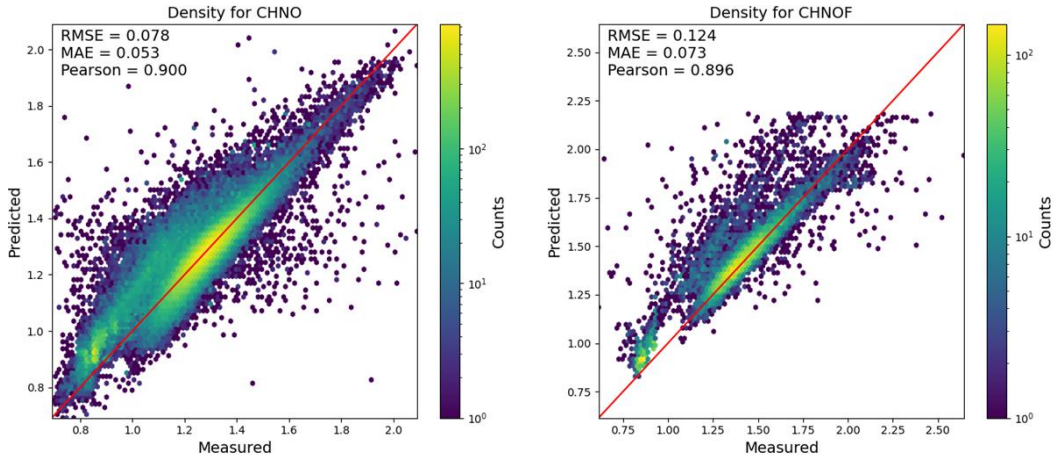

Figure 4. Comparison of measured and predicted crystalline density (g/cm^3) for CHNO (left) and CHNOF (right).

3.4 Detonation Velocity

Detonation velocity is one of the most useful properties for evaluating an energetic material (Appleton et al. 2025b). The left panel of Figure 5 shows that for CHNO, EPPI does well for materials with measured shock velocities over 6 km/s. Unfortunately, it appears to systematically overpredict the detonation velocity for materials with measured velocities below 6 km/s. This makes it difficult to use EPPI to discriminate between materials likely to have good performance and those with weak performance. The right panel of Figure 5 for CHNOF materials looks

considerably better; however, the dataset only spans the range of measured velocities above 6 km/s, and the lowest three values correspond to overpredicted values, implying the same problem with low-velocity predictions. Perhaps further training with lower velocity materials will improve its discriminatory power.

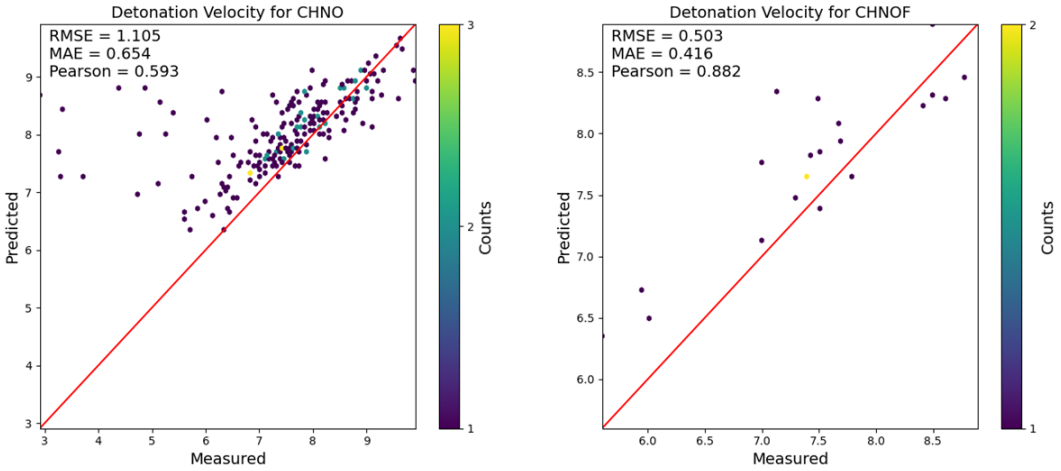

Figure 5. Comparison of measured and predicted detonation velocity (km/s) for CHNO (left) and CHNOF (right).

3.5 Detonation Pressure

Detonation pressure, like detonation velocity, is important for predicting energetic material performance (Appleton et al. 2025b). Here, a similar situation to what is seen with detonation velocity can be inferred but is not nearly as obvious. The lowest pressure materials all have overpredicted detonation pressures for CHNO materials—not only overpredicted but inversely correlated. However, the CHNOF panel (Figure 6, right) shows the lowest pressure material, lower than the lowest of the CHNO materials, and its predictions are very good. But this low-pressure CHNOF material was included in the training material and therefore seems likely that the low-pressure error for CHNO materials is due to underrepresentation of lower pressure materials in the training sets. EPPI predicts the values are very close to the measured values for the four materials containing fluorine. Evaluation of EPPI's predictive power for the detonation pressure may benefit from further study.

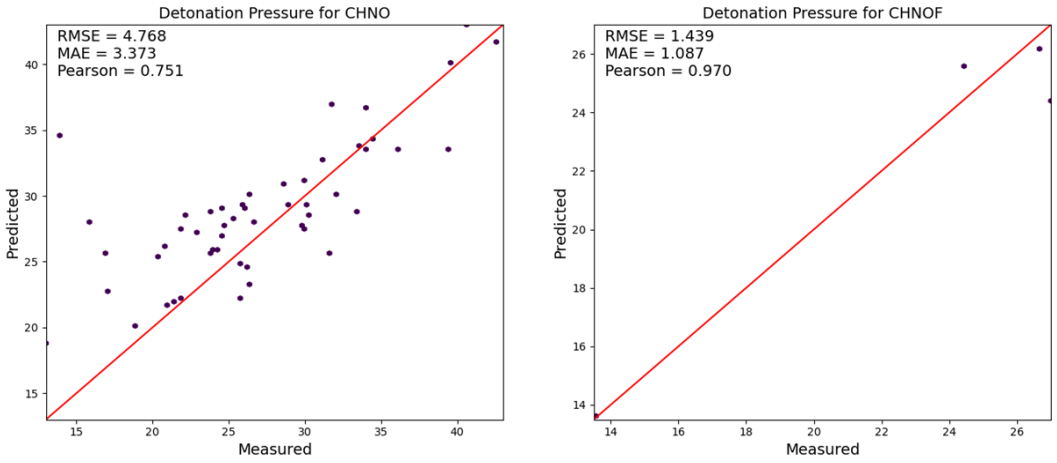

Figure 6. Comparison of measured and predicted detonation pressure (GPa) for CHNO (left) and CHNOF (right).

3.6 Impact Sensitivity (H_{50}[cm])

Impact sensitivity is both a very important measure of safety for a material and a difficult property to predict; EPPI employs two different ensemble models to evaluate it. The results reported herein are more accurate than those reported in the report describing the model (Lansford et al. 2022), as that work reported only results for the model that was not trained on the specific molecule whereas we are reporting the results for the ensemble, which should be better. Many of the measurements appear on the same vertical line due to the limited resolution of the experimental data (Figure 7). The experimentalists must do multiple drops at each height to get statistics on how likely the sample is to react, yet performing so many tests from very similar heights is not often feasible, thus some standard heights may be used.

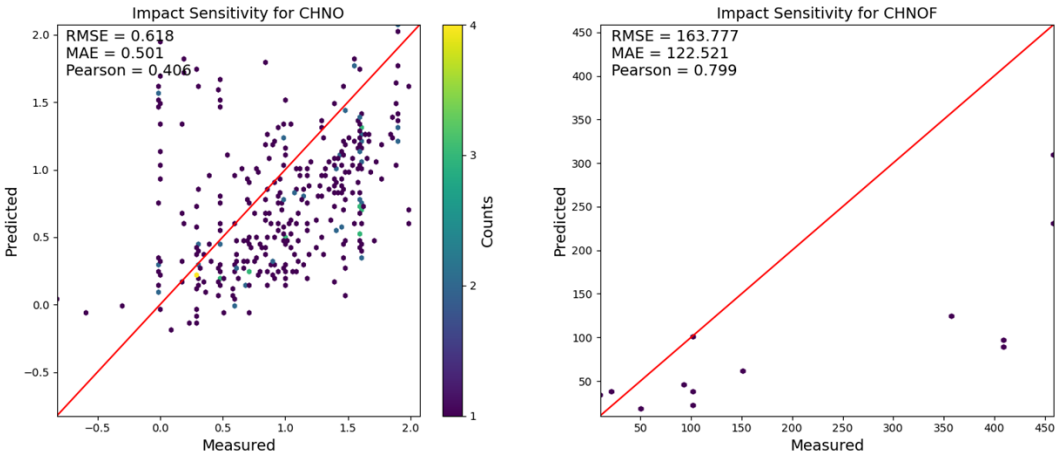

Figure 7. Comparison of measured and predicted impact sensitivity for CHNO (left) and CHNOF (right).

3.7 Impact Sensitivity (H_{50}log[J])

Here, the RA H_{50} model (Appleton et al. 2025c) is being evaluated. The impact sensitivity (H_{50}) here is given in the log of the impact energy. Given the noise in the experimental data, the EPPI predictions seem to be quite reasonable (Figure 8).

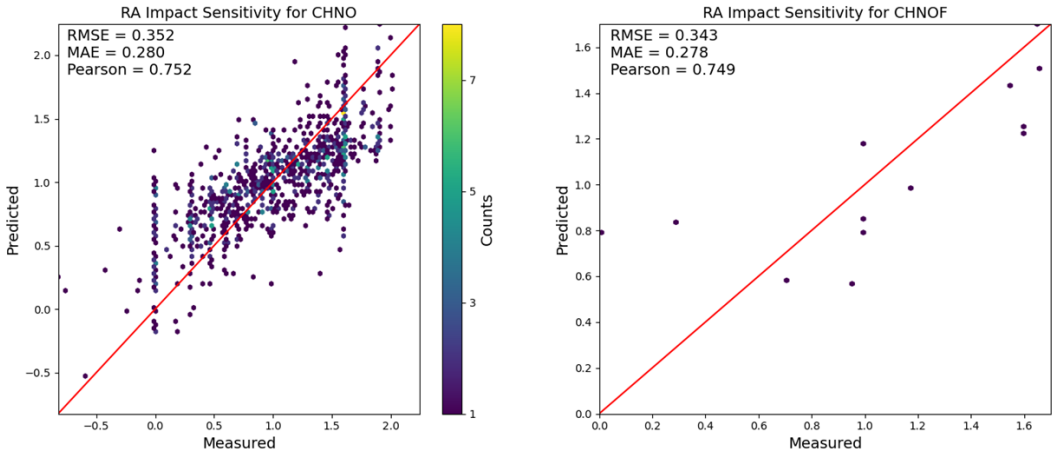

Figure 8. Comparison of measured and predicted impact sensitivity (H_{50}) in log(J) for CHNO (left) and CHNOF (right).

3.8 Melting Point (RA)

The melting point is important for estimating the safe temperatures for processing and storage of energetic materials. Figure 9 shows the agreement for CHNO materials for the Appleton melting point is excellent (Appleton et al. 2026). The agreement for CHNOF materials is not quite as good but still very reasonable.

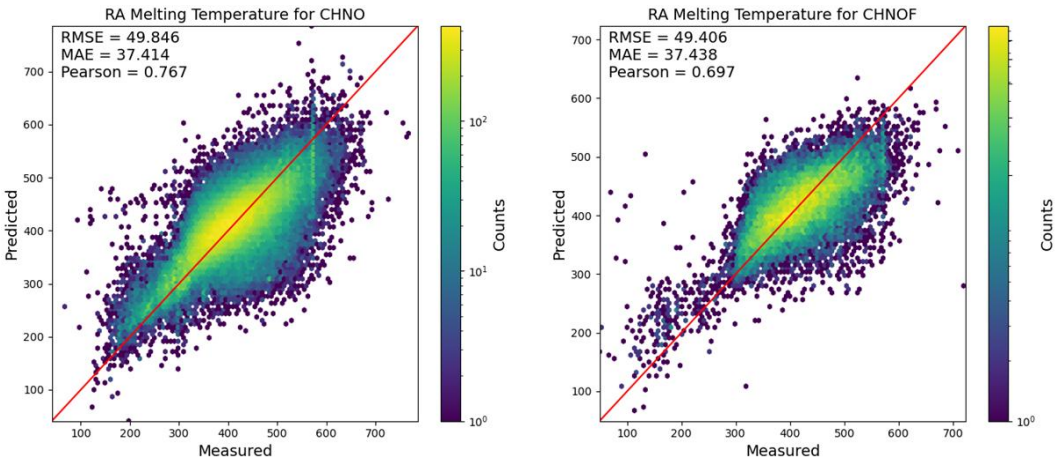

Figure 9. Comparison of measured and predicted melting temperature (K) for CHNO (left) and CHNOF (right).

3.9 Melting Point

The agreement for CHNO materials is excellent for the Lansford model (Lansford and Barnes 2025) (Figure 10), considerably better than the Appleton model. Similarly, the agreement for CHNOF materials is not quite as good as CHNO but still very reasonable and better than the Appleton model.

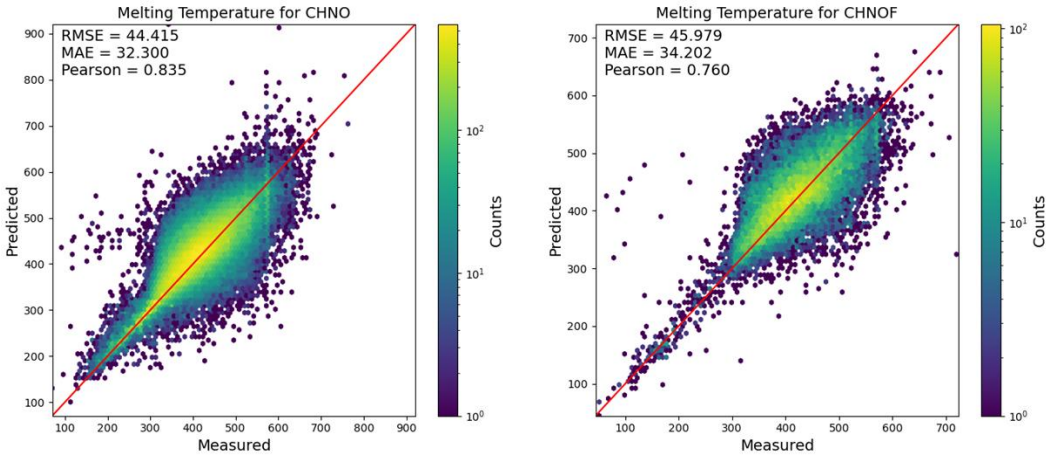

Figure 10. Comparison of measured and predicted melting temperature (K) for CHNO (left) and CHNOF (right).

3.10 Boiling Point

The boiling point is also useful for safety estimates (Lansford and Barnes 2025). It can be seen in Figure 11 that the agreement between EPPI and experiment is excellent for both CHNO and CHNOF datasets. The high temperature tails of both datasets start to diverge from the excellent correlation seen at lower temperatures, and this is not unexpected as the values in a dataset start to exceed the range of the training data. It is not clear that there is anything meaningful in the fact that the two datasets diverge in opposite directions; it is likely an artifact of the training.

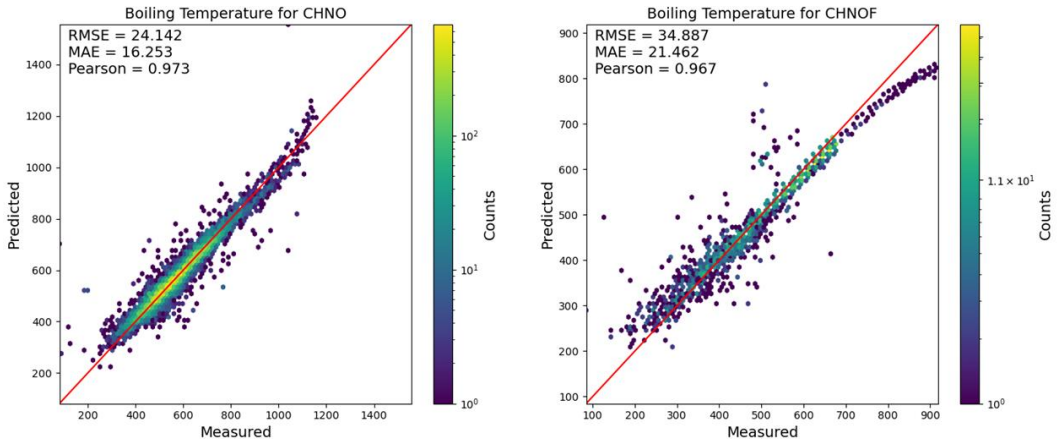

Figure 11. Comparison of measured and predicted boiling temperature (K) for CHNO (left) and CHNOF (right).

3.11 Decomposition Temperature

The final temperature prediction is for the decomposition temperature (Lansford and Barnes 2025). This is again a useful indicator for safe handling and storage. It is shown in Figure 12 that EPPI's predictions are reasonable for CHNO materials, particularly below approximately 600 K where a similar drift to that seen in the boiling temperature can be observed. There are only two data points in the CHNOF dataset, and they are near the upper left-hand corner (Figure 12), as EPPI significantly overpredicts the temperature. While the model gets the measured ordering correct in the CHNOF subset, there are only two data points and statistics such as Pearson correlation coefficient are not meaningful.

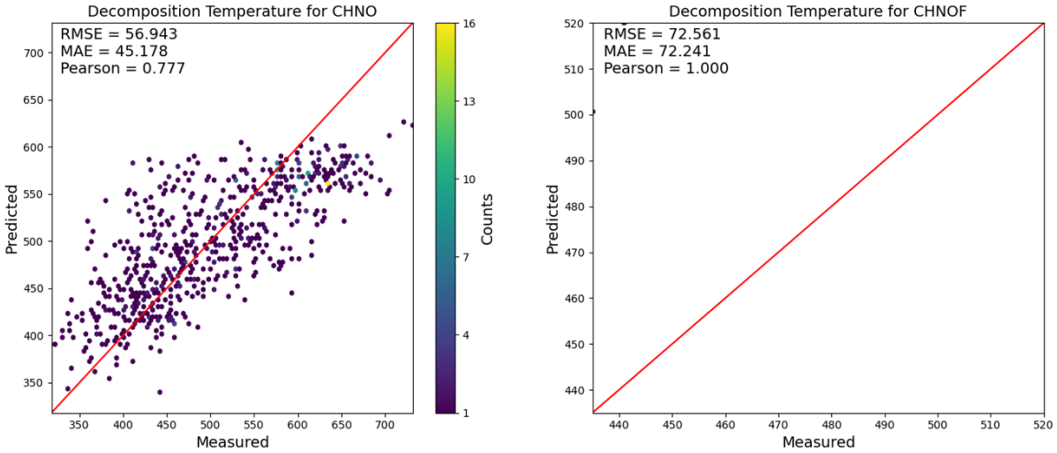

Figure 12. Comparison of measured and predicted decomposition temperature (K) for CHNO (left) and CHNOF (right).

3.12 Vapor Pressure

The final property being examined is vapor pressure (Lansford et al. 2023), which is another safety indicator (particularly for manufacturing). The logarithm of the vapor pressure is what is being calculated here, as the range of vapor pressure is very large. Additionally, the predicted vapor pressure is at 400 K while the experimental temperature varies with the particular experiment. Figure 13 shows that while EPPI slightly underpredicts the vapor pressure, the agreement is very good for both CHNO and CHNOF datasets with more dispersion at very low pressures, which is to be expected as the precision of the experiments becomes much harder at such small values of the log of the vapor pressure.

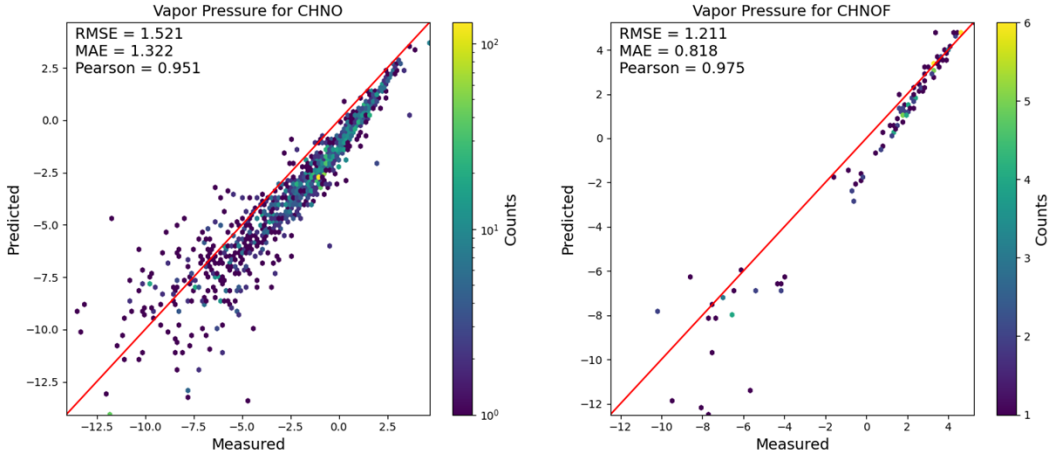

Figure 13. Comparison of measured and predicted vapor pressure in log(atm) for CHNO (left) and CHNOF (right).

4. Conclusions

In this work a large dataset of molecules has been curated containing some combination of carbon, nitrogen, oxygen, fluorine, and hydrogen with various properties relevant to energetic materials. These molecules have been run through EPPI and its predictions compared with experimental data are detailed. We found that EPPI does well at predicting most properties for CHNO materials and areas for future improvement have been identified, specifically for materials with extremely low detonation velocities and materials with high melting, boiling, and decomposition temperatures. The agreement with experiment is also quite good for CHNOF materials, particularly considering that these were not a focus of the model training—with the exceptions of decomposition temperature, where there is too little CHNOF data to make a meaningful conclusion, and the HoFs, which seemed systematically high. The extension to testing with fluorine materials suggests that EPPI can be used qualitatively outside of its primary training range and with some

additional training it may provide excellent results for materials of interest to the energetics community beyond those initially studied. Instructions and details about working with EPPI have also been provided as a guide for users, and suggestions for improvements have been made.

6. References

Appleton RJ et al. Interpretable performance models for energetic materials using parsimonious neural networks. J Phys Chem A. 2024;128(6):1142–1153. https://doi.org/10.1021/acs.jpca.3c06159

Appleton RJ et al. Multi-task multi-fidelity learning of properties for energetic materials. Prop Explos Pyrotech. 2025b;50:e202400248. https://doi.org/10.1002/prep.202400248

Appleton RJ, Barnes BC, Son SF, Strachan A. A deep learning approach to searching property spaces of materials. Digital Discovery. 2026;5(5):2172–2183. https://doi.org/10.1039/d5dd00422e

Appleton RJ, Barnes BC, Strachan A. Data fusion of deep learned molecular embeddings for property prediction. J Chem Inf Model. 2025a;65(21):11620–11630.

Byrd EFC. Simple computation of the heat of formation and density from theoretically predicted values. Army Research Laboratory (US); 2012. Report No.: ARL-TR-6206.

Chithrananda S, Grand G, Ramsundar B. Chemberta: large-scale self-supervised pretraining for molecular property prediction. arXiv; 2020. arXiv:2010.09885.

Frenkel M et al. ThermoML─an XML-based approach for storage and exchange of experimental and critically evaluated thermophysical and thermochemical property data. 1. Experimental data. J Chem Eng Data. 2003;48(1):2–13. https://doi.org/10.1021/je025645o

Fried L, Souers P. CHEETAH: a next generation thermochemical code. 1994. https://doi.org/10.2172/95184

Gilmer J, Schoenholz SS, Riley PF, Vinyals O, Dahl GE. Neural message passing for quantum chemistry. In: Proceedings of the 34th International Conference on Machine Learning; 2017; Sydney, Australia. PMLR 70; c2017.

Handley CA, Lambourn BD, Whitworth NJ, James HR, Belfield WJ. Understanding the shock and detonation response of high explosives at the continuum and meso scales. Appl Phys Rev. 2018;5:011303.

Heid E et al. Chemprop: a machine learning package for chemical property prediction. J Chem Inf Model. 2024;64:9−17.

Honda S, Shi S, Ueda HR. Smiles transformer: pre-trained molecular fingerprint for low data drug discovery. arXiv; 2019. arXiv:1911.04738.

Lansford JL, Barnes BC. Optimization of a graph-to-graph translation generative model under multiple constraints: discovering new melt-cast explosives. Prop Explos Pyrotech. 2025;50(11–12):e70043. https://doi.org/10.1002/prep.70043

Lansford JL, Barnes BC, Rice BM, Jensen KF. Building chemical property models for energetic materials from small datasets using a transfer learning approach. J Chem Inf Model. 2022;62(22):5397-5410. https://doi.org/10.1021/acs.jcim.2c00841

Lansford JL, Jensen KF, Barnes BC. Physics-informed transfer learning for out-of-sample vapor pressure predictions. Prop Explos Pyrotech. 2023;48: e202200265.

Muravyev NV, Wozniak DR, Piercey DG. Progress and performance of energetic materials: open dataset, tool, and implications for synthesis. J Mater Chem A. 2022;10:11054−11073.

Nieto-Draghi C et al. A general guidebook for the theoretical prediction of physicochemical properties of chemicals for regulatory purposes. Chem Rev. 2015;115:13093−13164.

Rae PJ, Dickson PM. Some observations about the dropweight explosive sensitivity test. J Dyn Behav Mater. 2021;7:414−424.

RDKit: open-source cheminformatics software. https://www.rdkit.org; 2026.

Sen O, Rai NK, Diggs AS, Hardin DB, Udaykumar HS. Multi-scale shock-to-detonation simulation of pressed energetic material: a meso-informed ignition and growth model. J Appl Phys. 2018;124:085110.

[SMGICT] Subcommittee on the Materials Genome Initiative Committee on Technology. Materials Genome Initiative strategic plan. National Scient and Technology Council (US); 2021 Nov. https://www.mgi.gov/sites/mgi/files/MGI-2021-Strategic-Plan.pdf

Weininger D. SMILES, a chemical language and information system. 1. Introduction to methodology and encoding rules. J Chem Inf Comput Sci. 1988;28(1):31–36.

Winter B, Winter C, Schilling J, Bardow A. A smile is all you need: predicting limiting activity coefficients from SMILES with natural language processing. Digital Discovery. 2022;1:859−869.

Yan QL, Zeman S. Theoretical evaluation of sensitivity and thermal stability for high explosives based on quantum chemistry methods: a brief review. Int J Quantum Chem. 2013;113:1049−1061.

Appendix A. Substructures

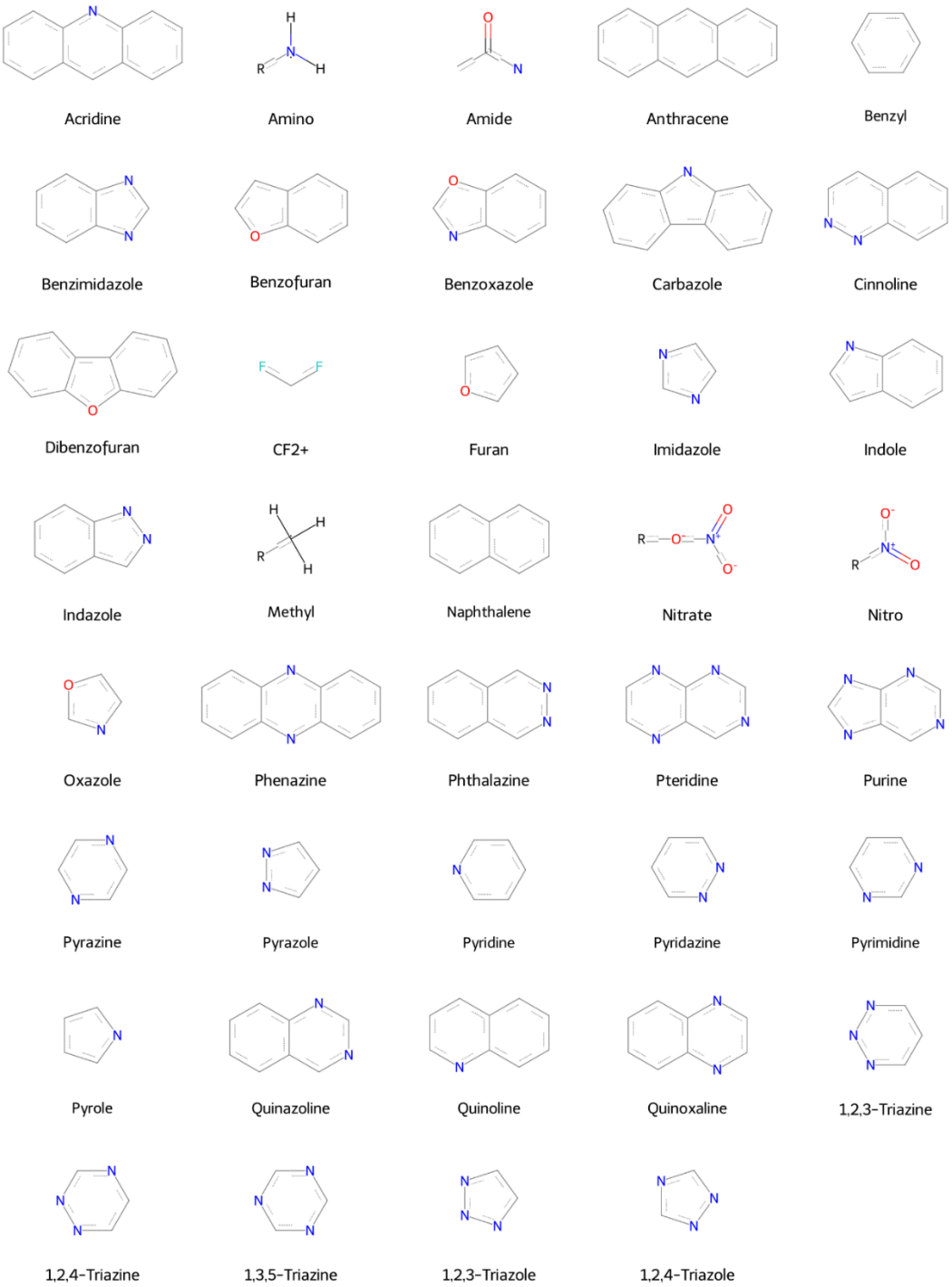

Figure A-1. 2D rendering of the molecular substructures used in assessing validation set coverage.

Appendix B. Distribution Details

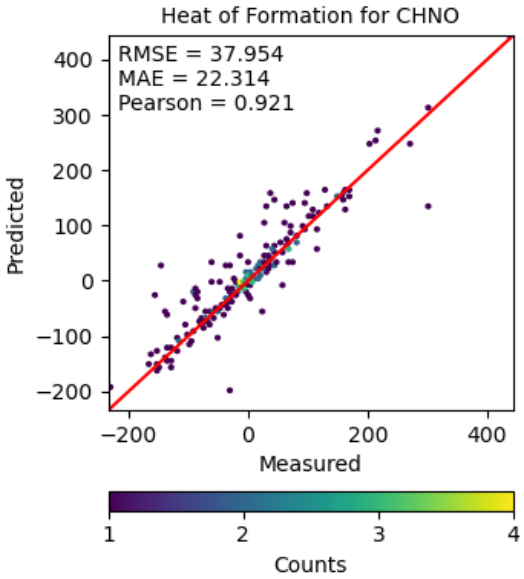

	Num	RMSE	MAE	Pearson
Amino	62	47.035	31.827	0.884
Amide	3	16.899	13.290	0.908
Benzyl	50	21.072	12.995	0.971
Imidazole	2	46.400	38.087	-1.000
Methyl	27	15.170	7.724	0.931
Naphthalene	1	2.602	2.602	nan
Nitrate	44	41.650	27.754	0.762
Nitro	150	34.169	18.413	0.886
Pyrazine	1	22.331	22.331	nan
Pyrazole	4	22.412	19.834	0.956
Pyridine	11	18.293	13.888	0.918
Pyrimidine	1	15.195	15.195	nan
1,3,5-Triazine	5	45.779	42.801	0.984
1,2,3-Triazole	3	62.988	45.269	-0.686
1,2,4-Triazole	12	46.068	30.158	0.788
Total	206	37.954	22.314	0.921

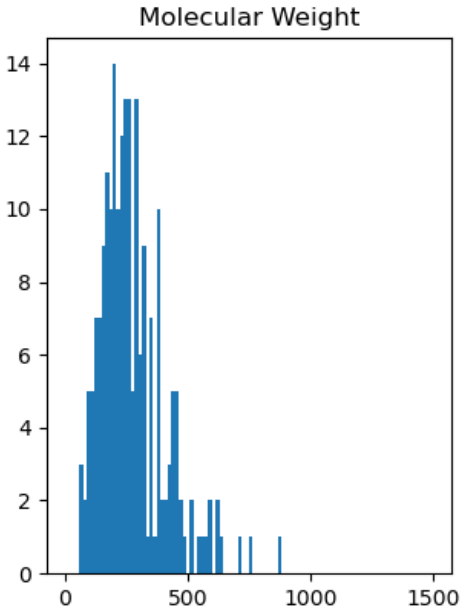

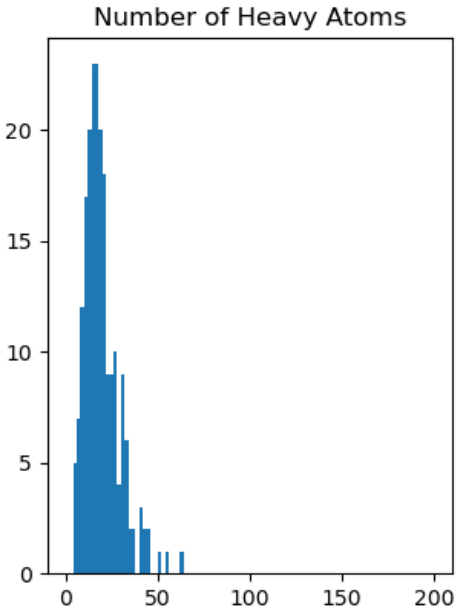

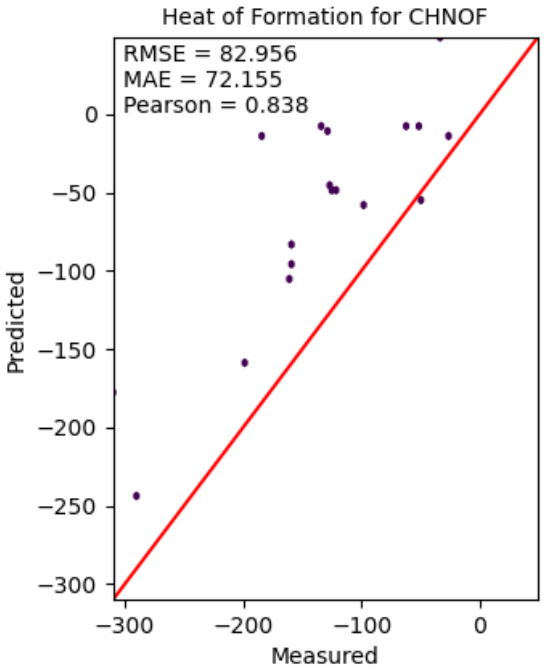

	Num	RMSE	MAE	Pearson
Benzyl	5	112.684	102.228	0.781
CF2+	3	143.617	142.396	0.973
Methyl	1	6.954	6.954	nan
Nitrate	1	39.848	39.848	nan
Nitro	16	87.900	79.858	0.874
Total	18	82.956	72.155	0.838

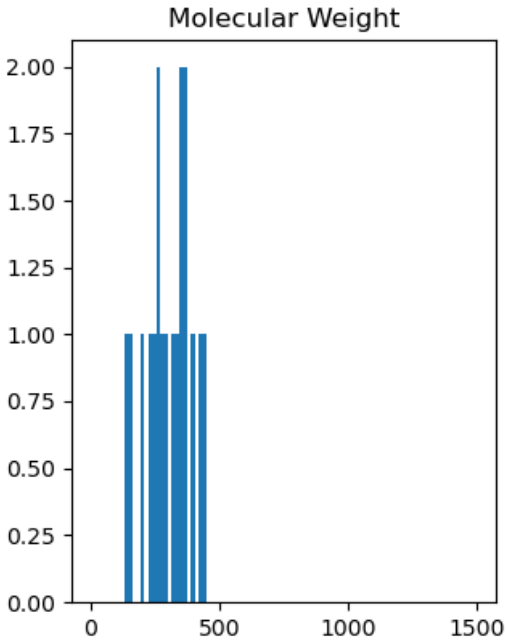

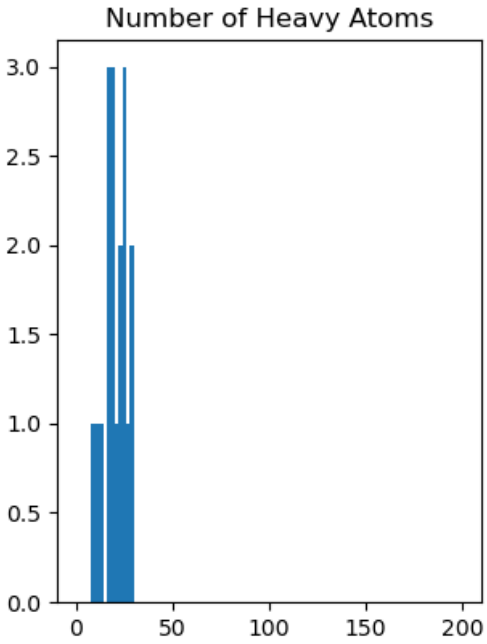

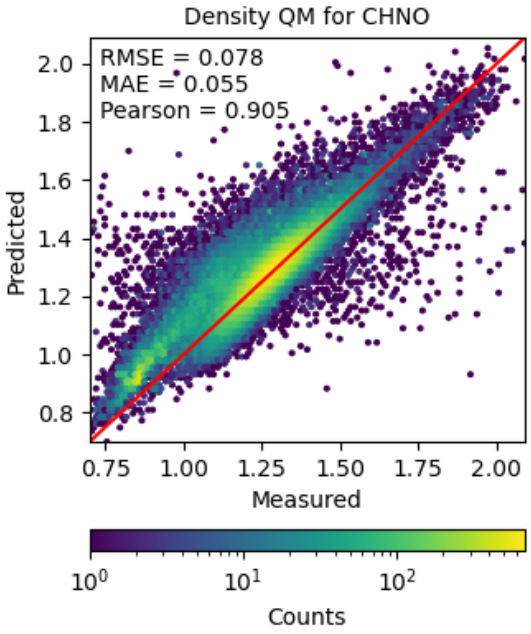

	Num	RMSE	MAE	Pearson
Amino	15021	0.083	0.059	0.897
Amide	22715	0.071	0.049	0.812
Anthracene	1203	0.112	0.071	0.495
Benzyl	84285	0.073	0.048	0.805
Benzofuran	812	0.073	0.048	0.758
Furan	2874	0.072	0.048	0.803
Imidazole	3217	0.082	0.054	0.810
Indole	4137	0.080	0.051	0.625
Methyl	98505	0.074	0.054	0.911
Naphthalene	8143	0.087	0.054	0.655
Nitro	9223	0.076	0.051	0.903
Purine	467	0.131	0.092	0.615
Pyrazine	1351	0.089	0.058	0.746
Pyrazole	2762	0.060	0.042	0.906
Pyridine	11297	0.071	0.047	0.786
Pyrimidine	2968	0.090	0.059	0.753
Pyrole	6939	0.080	0.050	0.689
Quinoline	2747	0.080	0.053	0.706
Quinoxaline	701	0.096	0.058	0.618
1,2,3-Triazole	1362	0.061	0.039	0.871
1,2,4-Triazole	1051	0.067	0.045	0.912
Total	129862	0.078	0.055	0.905

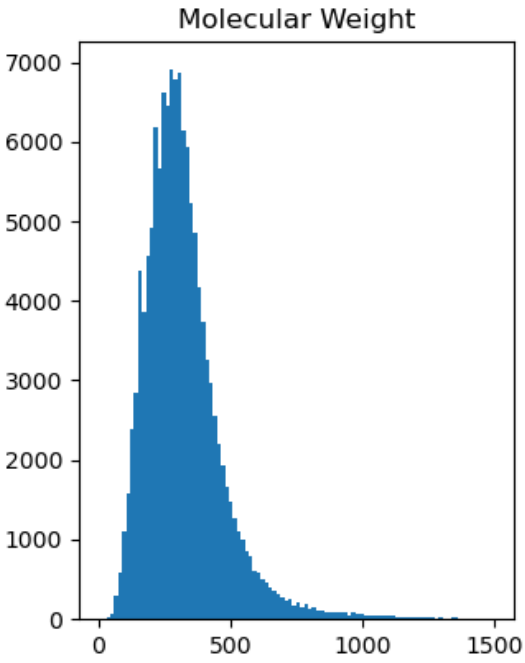

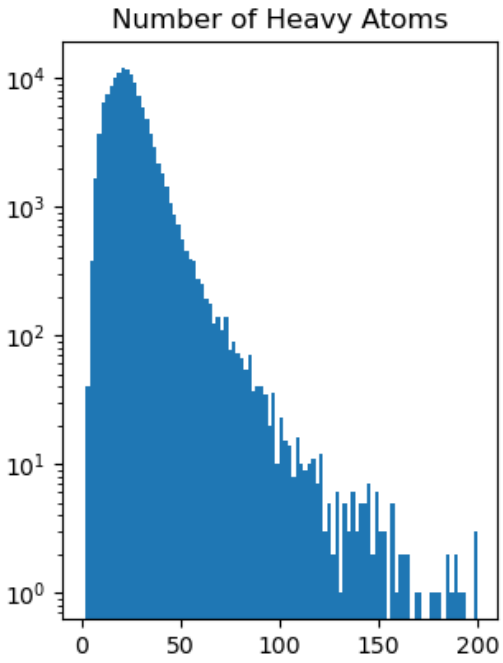

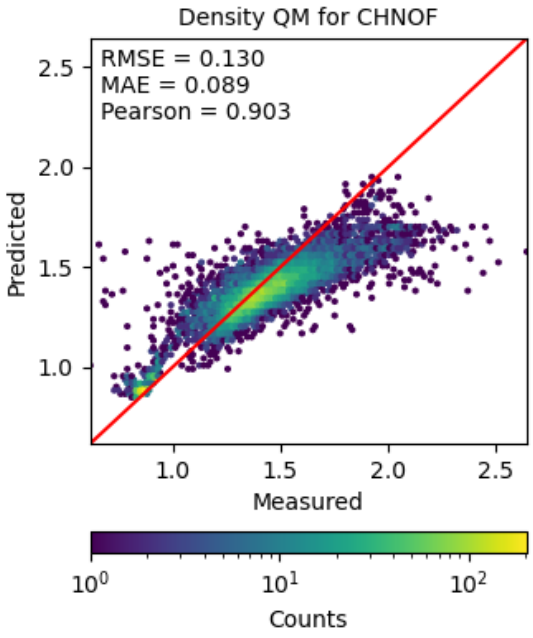

	Num	RMSE	MAE	Pearson
Amino	1413	0.124	0.088	0.773
Amide	2381	0.101	0.069	0.790
Anthracene	210	0.227	0.189	0.877
Benzyl	10073	0.127	0.089	0.794
CF2+	5653	0.155	0.110	0.819
Furan	185	0.121	0.086	0.805
Imidazole	337	0.112	0.076	0.771
Indole	389	0.100	0.070	0.707
Methyl	7649	0.091	0.065	0.940
Naphthalene	880	0.197	0.146	0.878
Nitro	742	0.105	0.073	0.852
Pyrazine	143	0.164	0.124	0.830
Pyrazole	378	0.127	0.084	0.790
Pyridine	1249	0.123	0.092	0.772
Pyrimidine	460	0.115	0.082	0.667
Pyrole	759	0.115	0.082	0.720
Quinoline	395	0.111	0.087	0.732
Quinoxaline	98	0.180	0.139	0.867
1,2,3-Triazole	176	0.095	0.070	0.863
1,2,4-Triazole	104	0.140	0.090	0.832
Total	13540	0.130	0.089	0.903

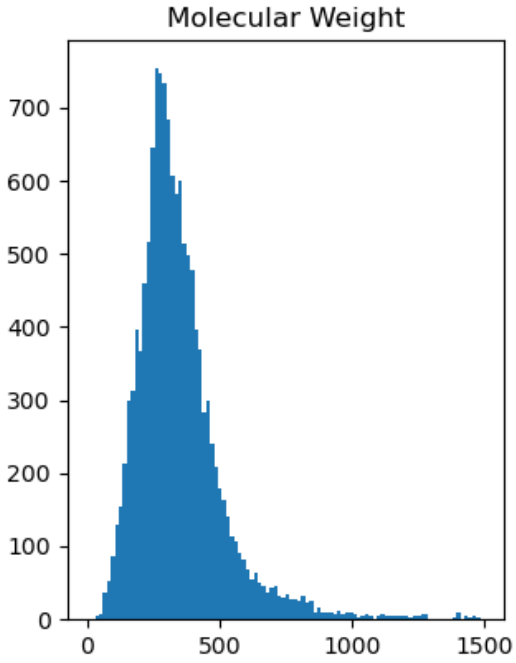

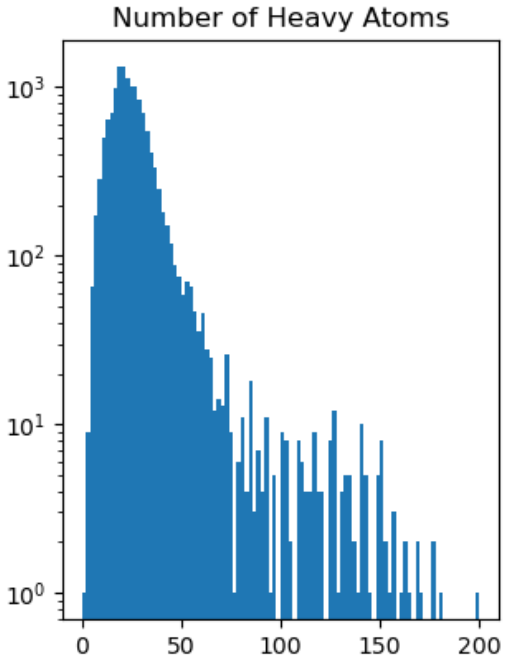

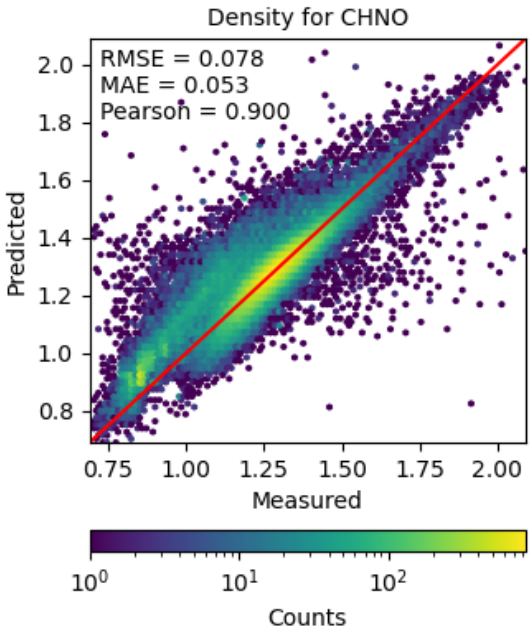

	Num	RMSE	MAE	Pearson
Amino	15021	0.080	0.054	0.899
Amide	22715	0.063	0.041	0.833
Anthracene	1203	0.117	0.070	0.478
Benzyl	84285	0.070	0.044	0.806
Benzofuran	812	0.072	0.045	0.761
Furan	2874	0.072	0.048	0.782
Imidazole	3217	0.074	0.047	0.831
Indole	4137	0.074	0.044	0.656
Methyl	98505	0.073	0.051	0.906
Naphthalene	8143	0.089	0.052	0.646
Nitro	9223	0.070	0.044	0.908
Purine	467	0.119	0.083	0.650
Pyrazine	1351	0.088	0.053	0.766
Pyrazole	2762	0.056	0.036	0.917
Pyridine	11297	0.071	0.044	0.790
Pyrimidine	2968	0.081	0.051	0.784
Pyrole	6939	0.074	0.044	0.714
Quinoline	2747	0.085	0.052	0.685
Quinoxaline	701	0.095	0.053	0.646
1,2,3-Triazole	1362	0.056	0.035	0.891
1,2,4-Triazole	1051	0.058	0.037	0.931
Total	129862	0.078	0.053	0.900

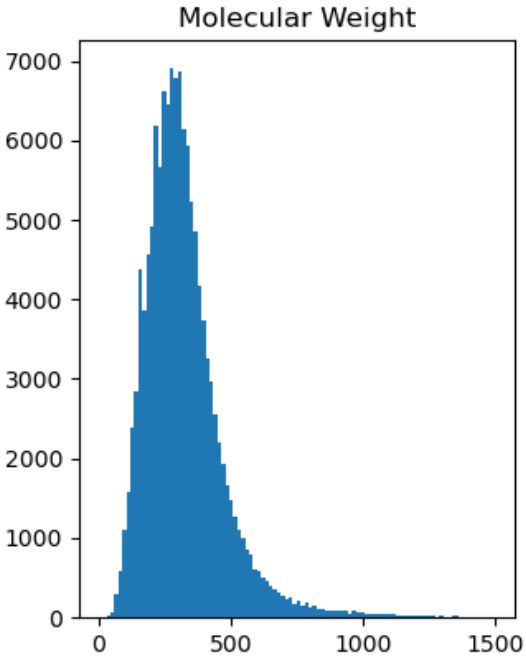

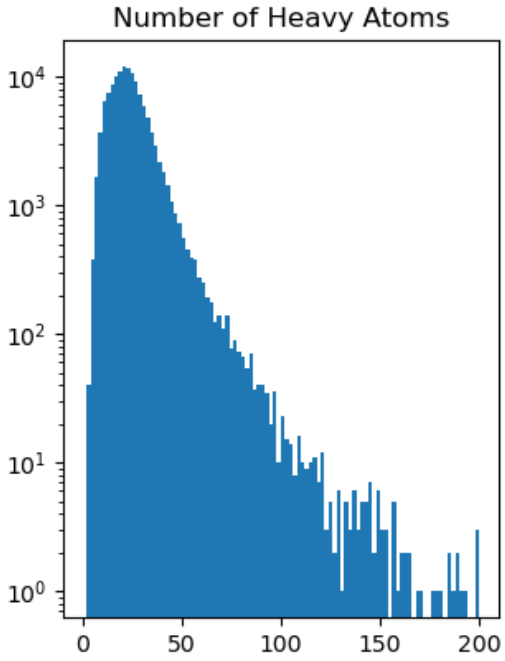

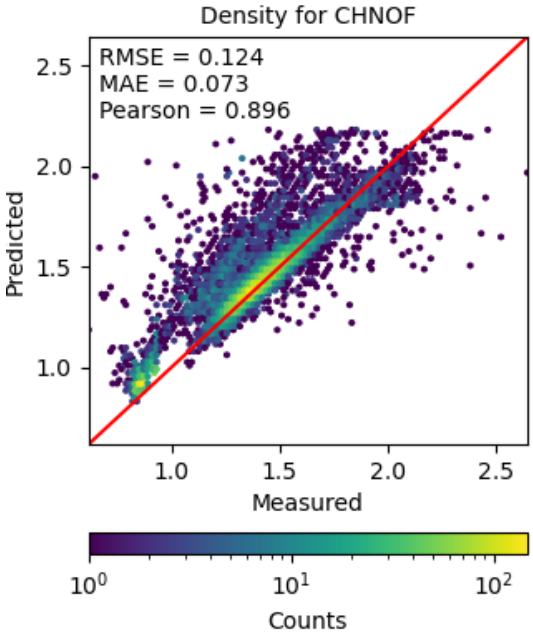

	Num	RMSE	MAE	Pearson
Amino	1413	0.105	0.065	0.840
Amide	2381	0.076	0.046	0.865
Anthracene	210	0.164	0.110	0.891
Benzyl	10073	0.101	0.059	0.840
CF2+	5653	0.147	0.084	0.769
Furan	185	0.077	0.047	0.867
Imidazole	337	0.082	0.047	0.863
Indole	389	0.081	0.049	0.822
Methyl	7649	0.097	0.062	0.933
Naphthalene	880	0.130	0.079	0.897
Nitro	742	0.098	0.058	0.859
Pyrazine	143	0.063	0.046	0.946
Pyrazole	378	0.087	0.047	0.873
Pyridine	1249	0.070	0.042	0.886
Pyrimidine	460	0.094	0.061	0.817
Pyrole	759	0.111	0.066	0.770
Quinoline	395	0.059	0.039	0.896
Quinoxaline	98	0.069	0.048	0.945
1,2,3-Triazole	176	0.040	0.033	0.958
1,2,4-Triazole	104	0.076	0.049	0.923
Total	13540	0.124	0.073	0.896

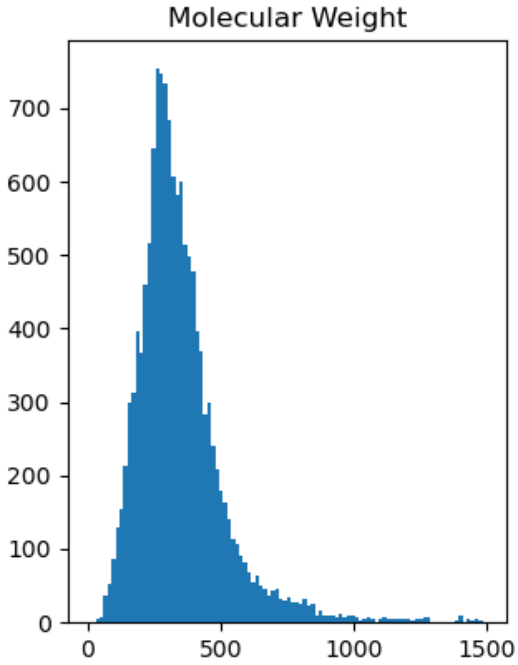

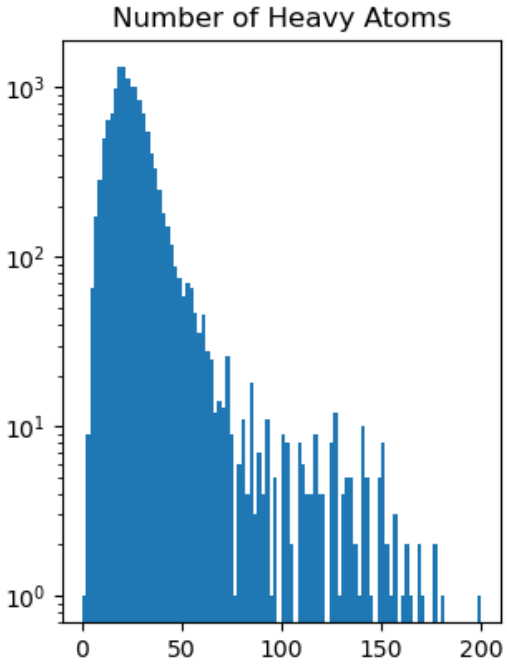

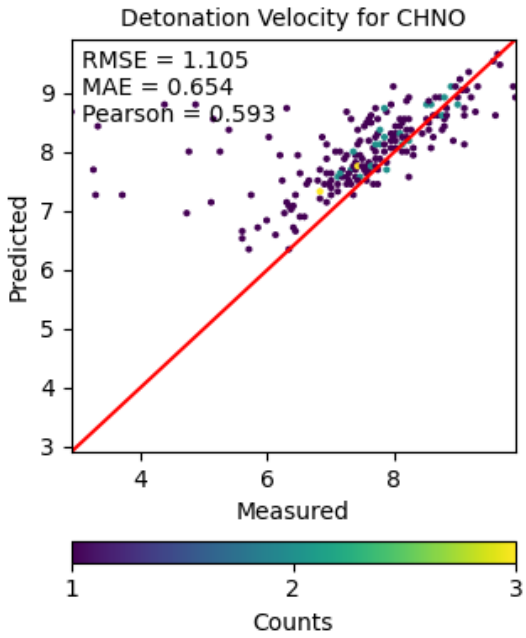

	Num	RMSE	MAE	Pearson
Amino	65	1.566	0.933	0.231
Amide	3	0.592	0.551	0.950
Benzyl	52	0.494	0.372	0.867
Imidazole	2	0.257	0.199	-1.000
Methyl	30	0.928	0.607	0.717
Naphthalene	1	0.214	0.214	nan
Nitrate	47	1.186	0.787	0.586
Nitro	158	0.799	0.493	0.674
Pyrazine	1	0.355	0.355	nan
Pyrazole	4	0.537	0.379	0.965
Pyridine	11	0.575	0.535	0.681
Pyrimidine	1	0.067	0.067	nan
1,3,5-Triazine	5	0.781	0.666	0.512
1,2,3-Triazole	3	0.515	0.437	0.998
1,2,4-Triazole	13	0.583	0.493	0.744
Total	218	1.105	0.654	0.593

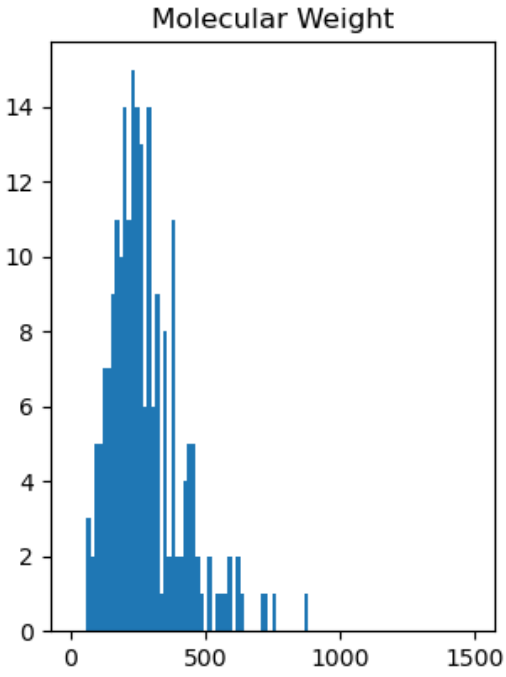

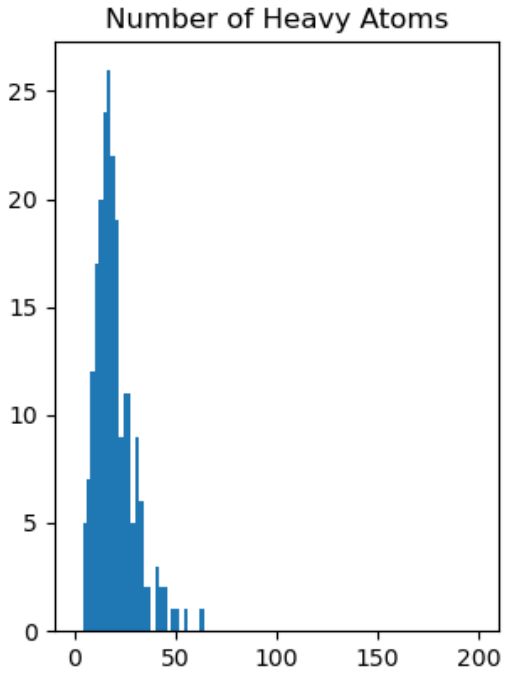

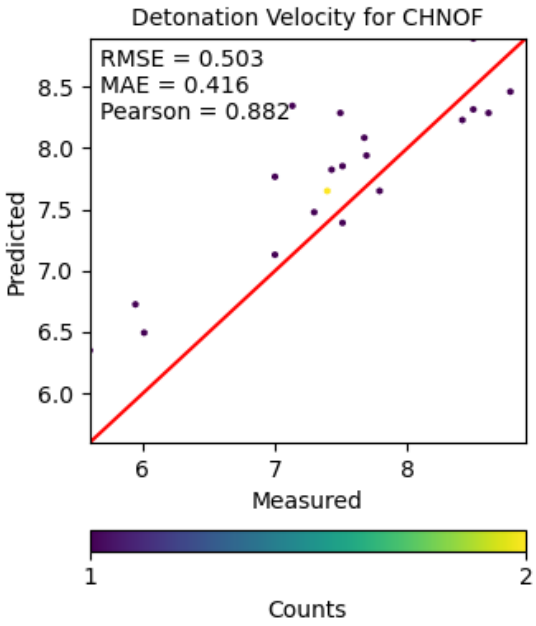

	Num	RMSE	MAE	Pearson
Benzyl	5	0.384	0.296	-0.325
CF2+	4	0.270	0.252	-0.793
Methyl	4	0.554	0.476	0.975
Nitrate	1	1.218	1.218	nan
Nitro	17	0.479	0.387	0.651
Total	21	0.503	0.416	0.882

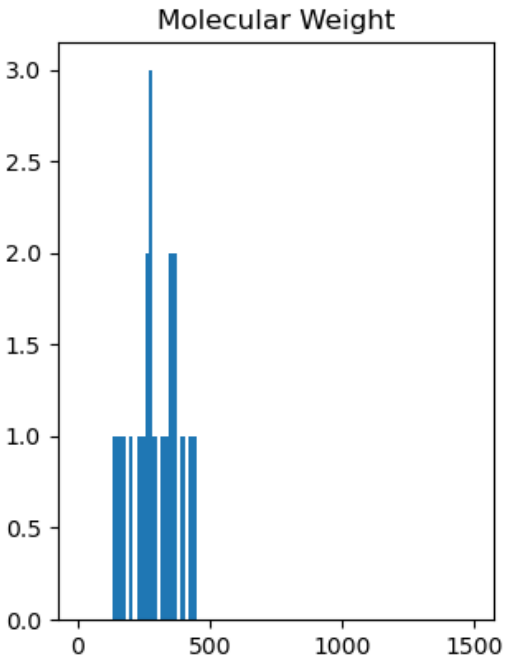

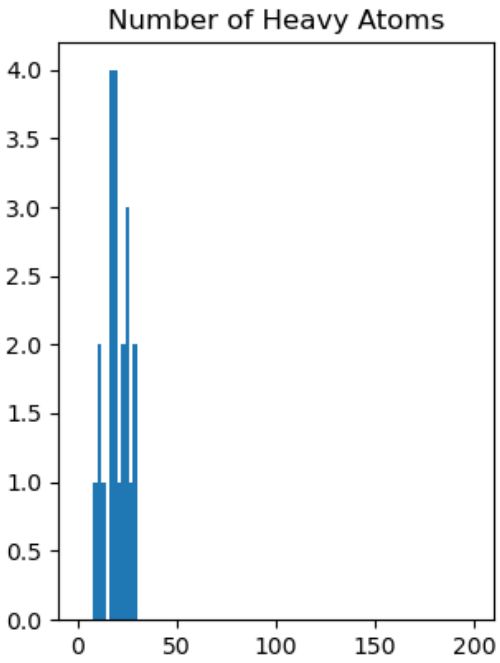

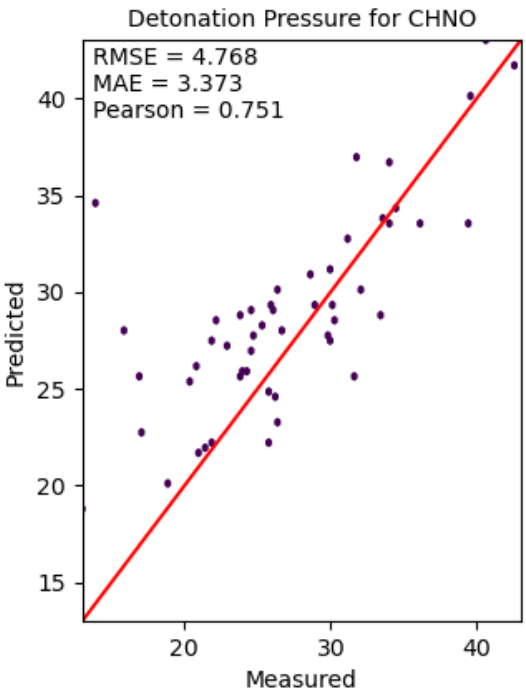

	Num	RMSE	MAE	Pearson
Amino	21	3.224	2.715	0.522
Benzyl	14	3.557	2.666	0.751
Methyl	5	3.978	3.450	0.901
Nitrate	5	3.566	3.086	0.711
Nitro	40	5.188	3.661	0.756
Pyrazine	1	1.938	1.938	nan
Pyrazole	2	1.163	1.044	-1.000
1,2,3-Triazole	1	3.042	3.042	nan
1,2,4-Triazole	5	3.234	3.156	0.307
Total	51	4.768	3.373	0.751

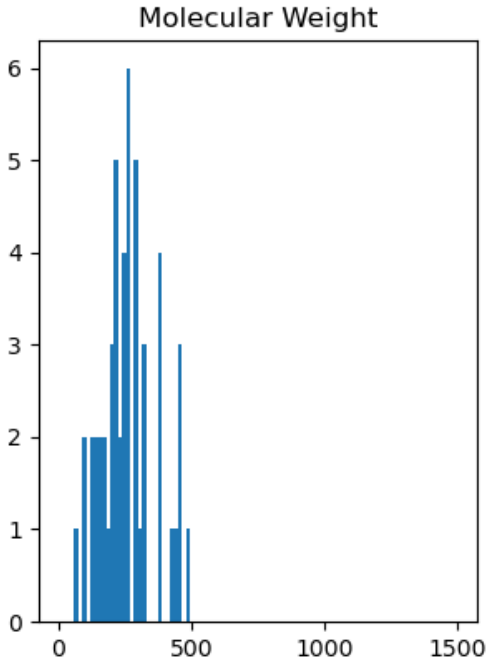

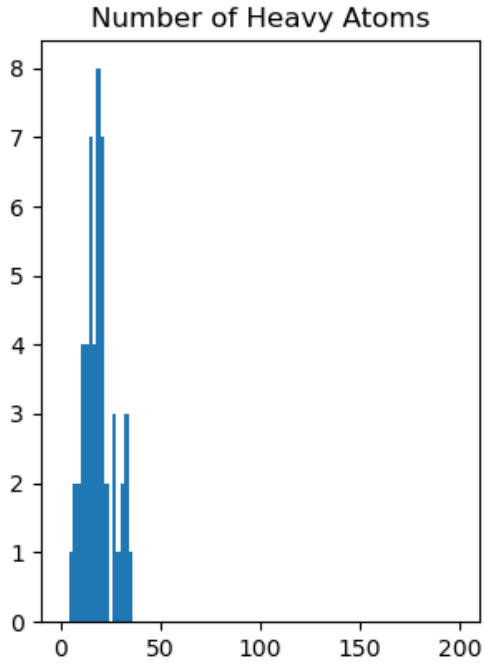

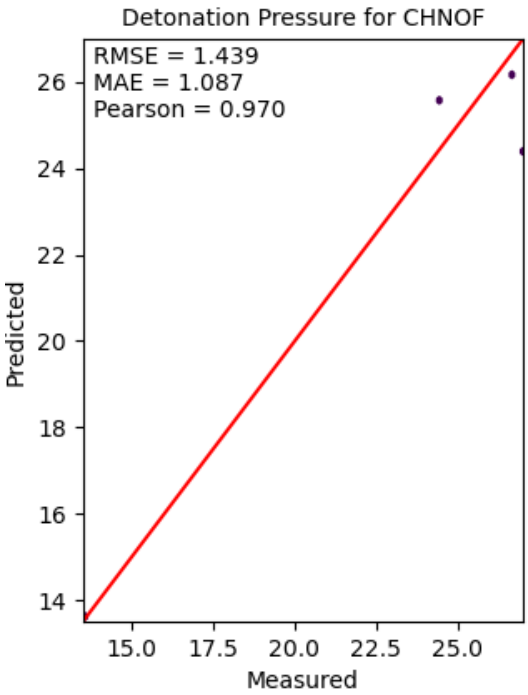

	Num	RMSE	MAE	Pearson
Benzyl	2	1.879	1.580	-1.000
Methyl	1	0.085	0.085	nan
Nitro	3	1.661	1.421	-0.323
Total	4	1.439	1.087	0.970

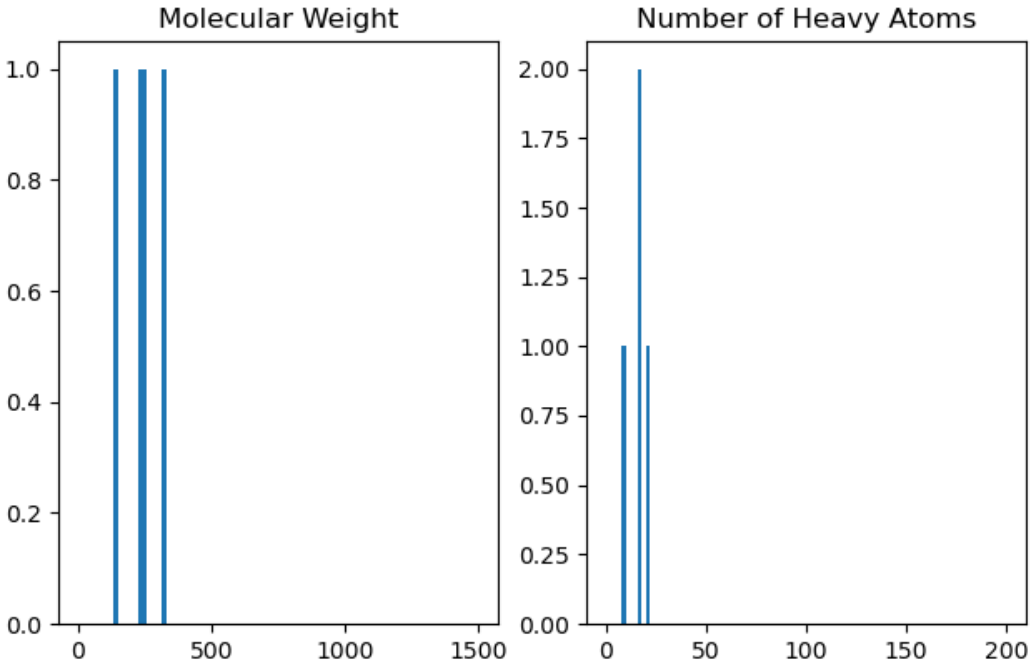

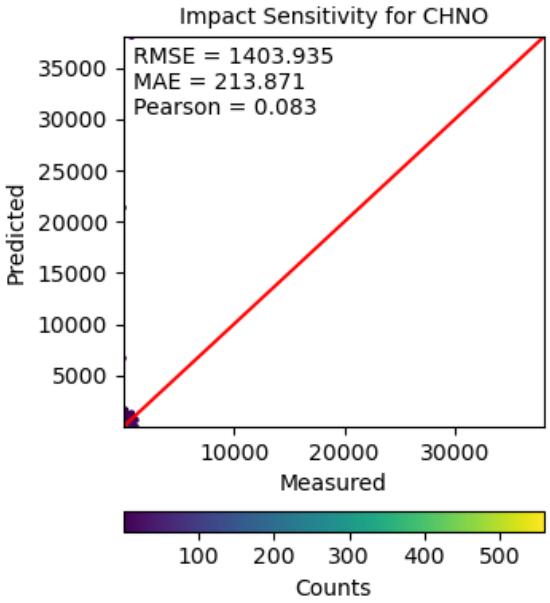

	Num	RMSE	MAE	Pearson
Amino	294	2198.715	302.511	0.117
Amide	28	136.724	99.423	0.915
Benzyl	204	261.539	176.158	0.153
Benzimidazole	2	224.638	178.373	-1.000
Imidazole	42	220.918	155.111	0.660
Methyl	219	2960.923	514.051	0.087
Naphthalene	1	166.727	166.727	nan
Nitrate	72	216.399	99.897	0.641
Nitro	778	1557.271	206.468	0.099
Pyrazine	3	216.920	191.194	0.944
Pyrazole	133	3253.415	429.701	0.194
Pyridine	10	55.166	43.949	0.872
Pyridazine	9	202.635	131.081	0.038
Pyrimidine	4	302.051	243.377	0.974
1,2,3-Triazine	3	265.165	265.138	0.997
1,2,4-Triazine	8	462.396	424.844	0.564
1,3,5-Triazine	5	200.392	183.927	0.552
1,2,3-Triazole	42	170.028	119.221	0.461
1,2,4-Triazole	120	257.061	182.061	0.247
Total	990	1403.935	213.871	0.083

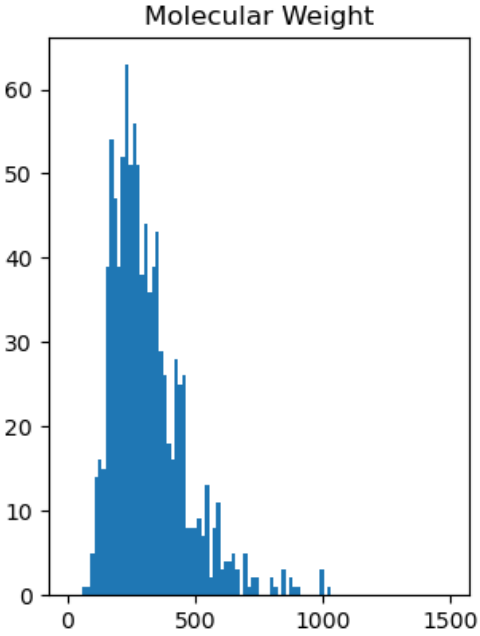

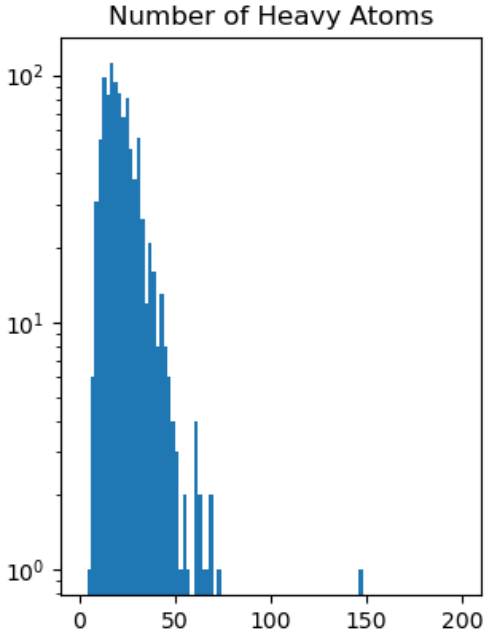

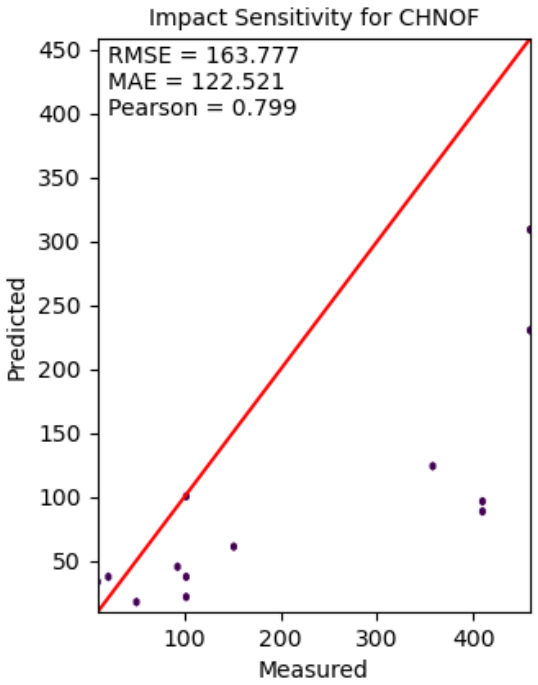

	Num	RMSE	MAE	Pearson
Benzyl	1	231.226	231.226	nan
CF2+	3	243.025	233.147	0.940
Methyl	4	251.040	221.210	0.852
Nitro	9	114.528	73.567	0.674
1,2,3-Triazole	4	240.129	232.667	0.783
Total	13	163.777	122.521	0.799

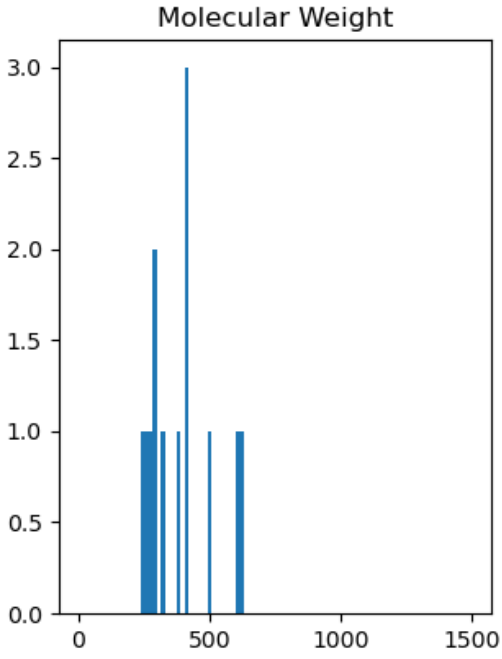

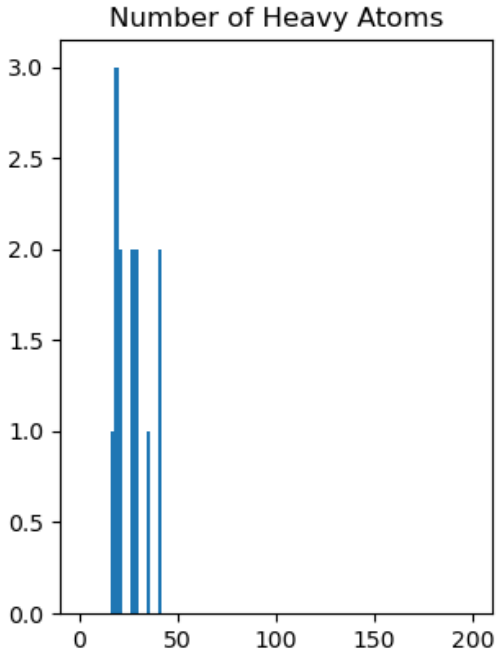

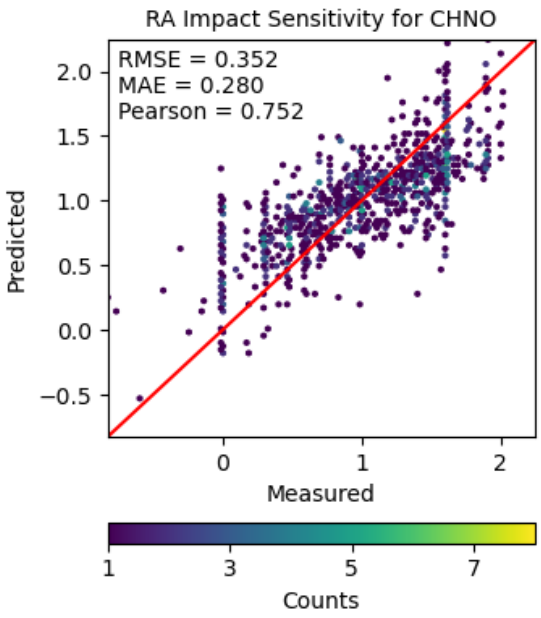

	Num	RMSE	MAE	Pearson
Amino	294	0.325	0.262	0.741
Amide	28	0.256	0.219	0.861
Benzyl	204	0.351	0.275	0.696
Benzimidazole	2	0.343	0.328	-1.000
Imidazole	42	0.319	0.247	0.832
Methyl	219	0.342	0.287	0.773
Naphthalene	1	0.207	0.207	nan
Nitrate	72	0.323	0.258	0.790
Nitro	778	0.339	0.272	0.727
Pyrazine	3	0.246	0.229	0.954
Pyrazole	133	0.317	0.257	0.727
Pyridine	10	0.146	0.121	0.880
Pyridazine	9	0.298	0.258	0.563
Pyrimidine	4	0.213	0.140	0.804
1,2,3-Triazine	3	0.175	0.136	0.969
1,2,4-Triazine	8	0.369	0.297	0.560
1,3,5-Triazine	5	0.330	0.282	0.833
1,2,3-Triazole	42	0.328	0.265	0.686
1,2,4-Triazole	120	0.419	0.330	0.633
Total	990	0.352	0.280	0.752

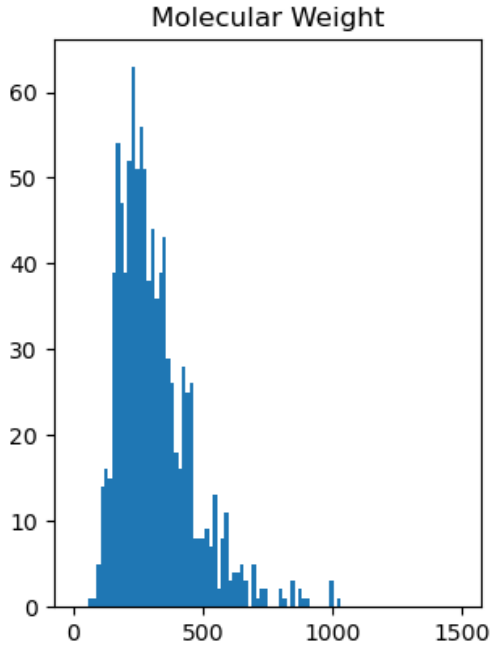

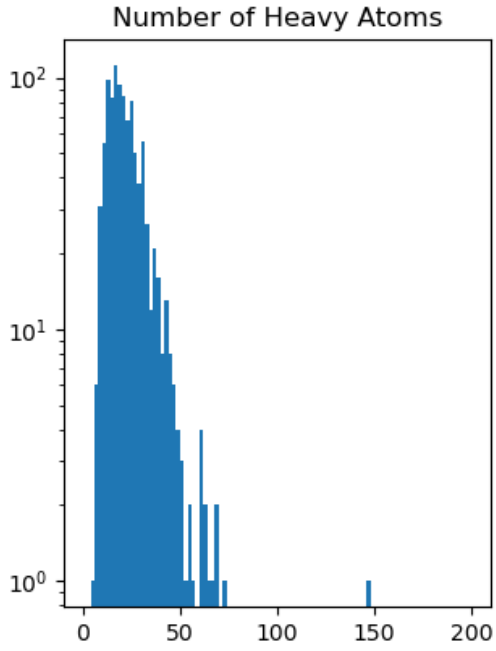

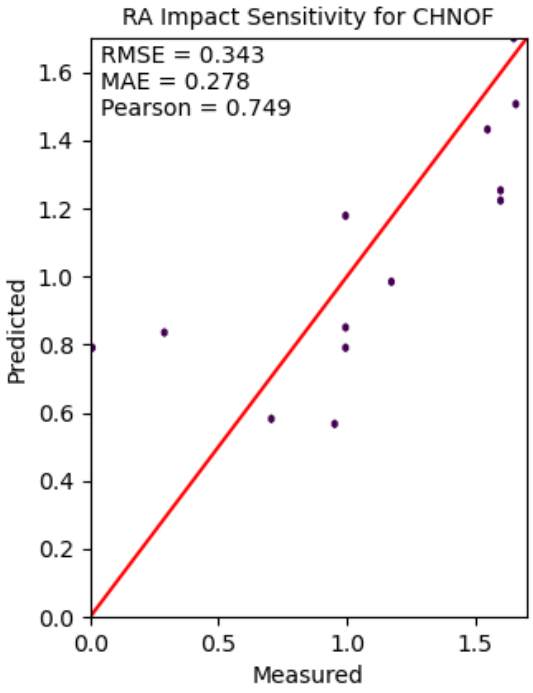

	Num	RMSE	MAE	Pearson
Benzyl	1	0.118	0.118	nan
CF2+	3	0.237	0.192	0.910
Methyl	4	0.476	0.409	0.932
Nitro	9	0.386	0.324	0.504
1,2,3-Triazole	4	0.213	0.174	0.529
Total	13	0.343	0.278	0.749

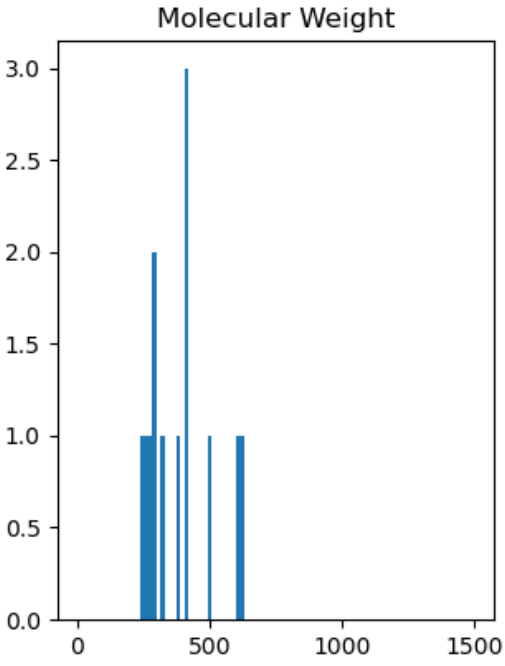

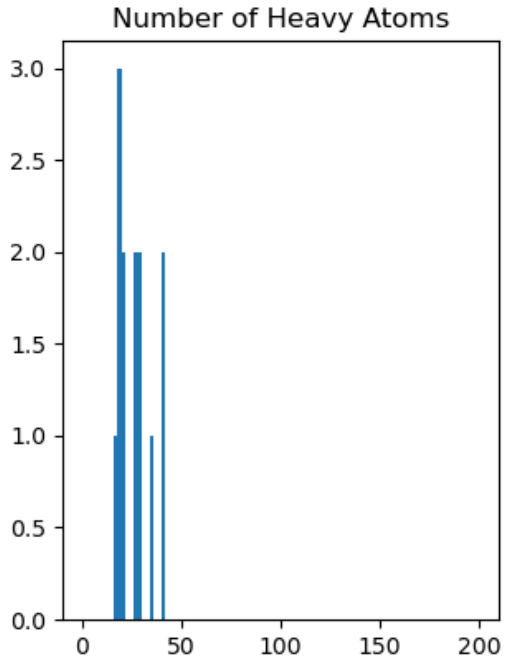

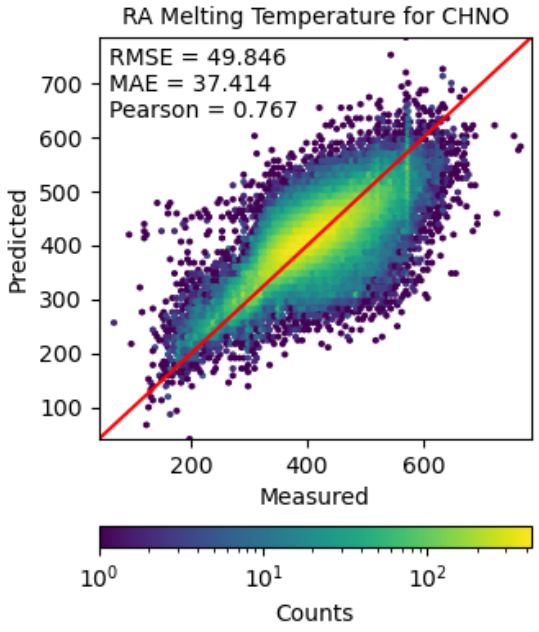

	Num	RMSE	MAE	Pearson
Amino	28866	53.264	40.334	0.665
Amide	33197	47.670	36.968	0.644
Benzyl	94865	47.741	36.403	0.690
Benzofuran	1576	43.700	33.732	0.696
Furan	3908	44.952	34.185	0.707
Imidazole	9785	48.899	38.285	0.668
Indole	5638	52.895	41.456	0.589
Methyl	99416	49.933	37.355	0.764
Naphthalene	4292	46.375	35.752	0.711
Nitro	8777	42.605	32.798	0.763
Oxazole	2338	38.848	29.667	0.735
Purine	1349	55.021	44.652	0.655
Pyrazine	1700	45.606	35.747	0.784
Pyrazole	7039	46.509	36.339	0.717
Pyridine	21392	48.506	37.832	0.687
Pyridazine	1999	46.690	35.950	0.655
Pyrimidine	9008	49.652	39.284	0.692
Pyrole	8760	51.500	39.969	0.637
Quinazoline	1554	47.342	37.412	0.691
Quinoline	5156	49.062	38.398	0.666
1,2,4-Triazole	2188	45.945	35.778	0.737
Total	131174	49.846	37.414	0.767

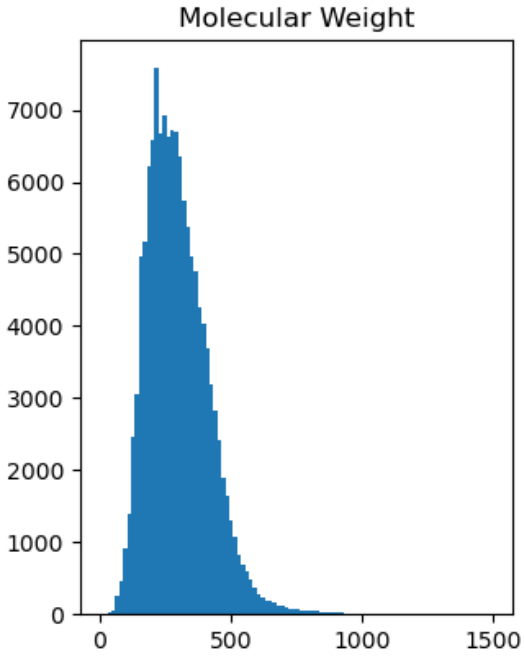

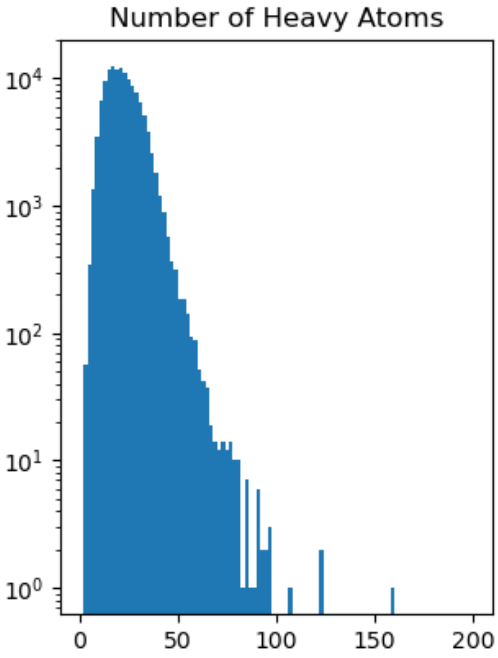

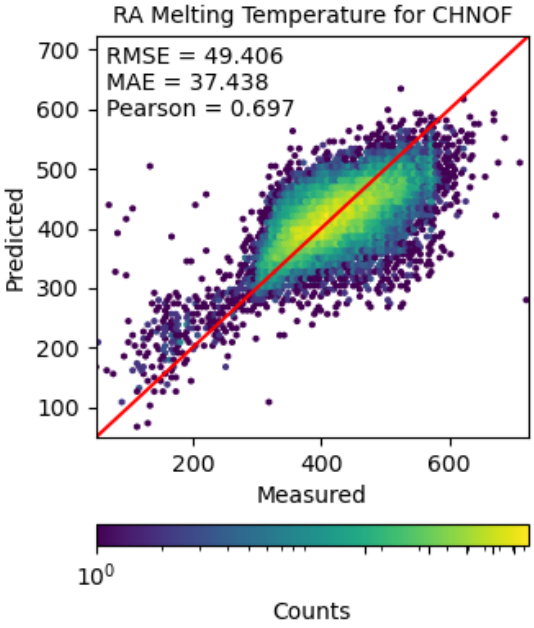

	Num	RMSE	MAE	Pearson
Amino	6228	52.577	39.950	0.589
Amide	8370	47.257	36.899	0.560
Benzyl	24488	47.926	36.594	0.661
CF2+	10994	48.932	37.031	0.695
Furan	612	44.054	33.768	0.656
Imidazole	1981	48.981	37.446	0.571
Indole	1180	50.904	40.138	0.522
Methyl	16251	50.136	38.066	0.652
Naphthalene	590	55.259	44.351	0.467
Nitro	1404	43.035	31.911	0.724
Oxazole	476	42.999	32.460	0.611
Pyrazine	329	47.836	38.755	0.759
Pyrazole	2625	41.452	32.253	0.734
Pyridine	6679	49.203	38.590	0.659
Pyridazine	701	43.127	34.095	0.627
Pyrimidine	2589	48.209	38.339	0.622
Pyrole	1894	49.637	39.224	0.603
Quinazoline	345	49.818	39.108	0.626
Quinoline	2256	55.294	44.781	0.508
1,2,3-Triazole	388	45.500	35.369	0.557
1,2,4-Triazole	860	42.827	33.569	0.695
Total	26813	49.406	37.438	0.697

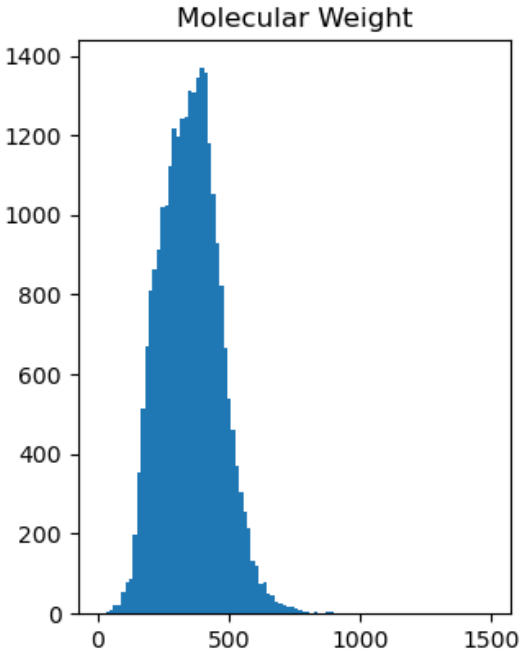

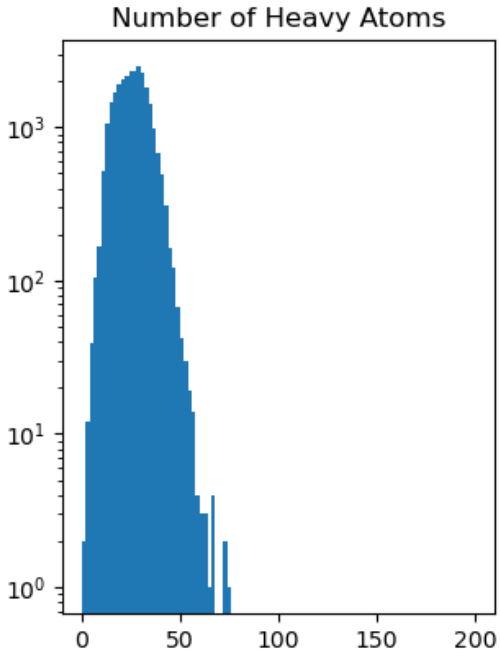

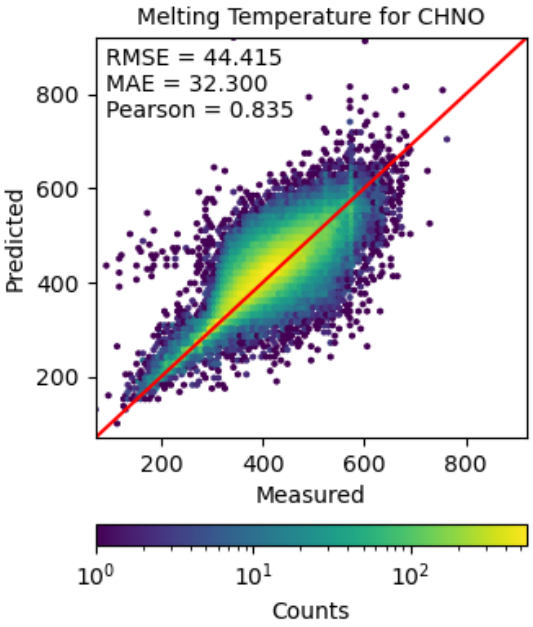

	Num	RMSE	MAE	Pearson
Amino	28866	51.487	38.429	0.719
Amide	33197	46.845	35.825	0.697
Benzyl	94865	46.359	34.638	0.744
Benzofuran	1576	47.311	37.399	0.742
Furan	3908	48.360	37.777	0.754
Imidazole	9785	52.928	40.570	0.684
Indole	5638	54.287	41.621	0.647
Methyl	99416	43.700	31.683	0.840
Naphthalene	4292	45.554	33.897	0.769
Nitro	8777	41.474	31.100	0.793
Oxazole	2338	45.774	35.783	0.724
Purine	1349	53.703	42.206	0.724
Pyrazine	1700	50.676	39.240	0.782
Pyrazole	7039	48.776	38.160	0.699
Pyridine	21392	49.497	37.984	0.721
Pyridazine	1999	47.936	36.734	0.643
Pyrimidine	9008	52.293	40.673	0.710
Pyrole	8760	53.949	41.197	0.675
Quinazoline	1554	55.491	43.289	0.685
Quinoline	5156	50.535	38.260	0.690
1,2,4-Triazole	2188	45.205	34.865	0.727
Total	131174	44.415	32.300	0.835

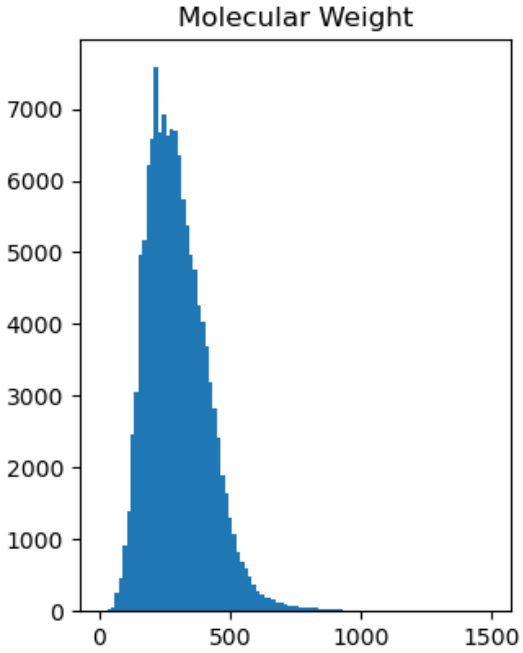

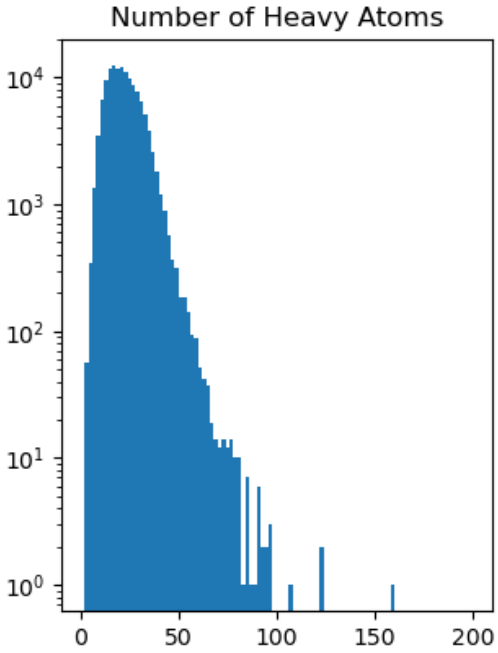

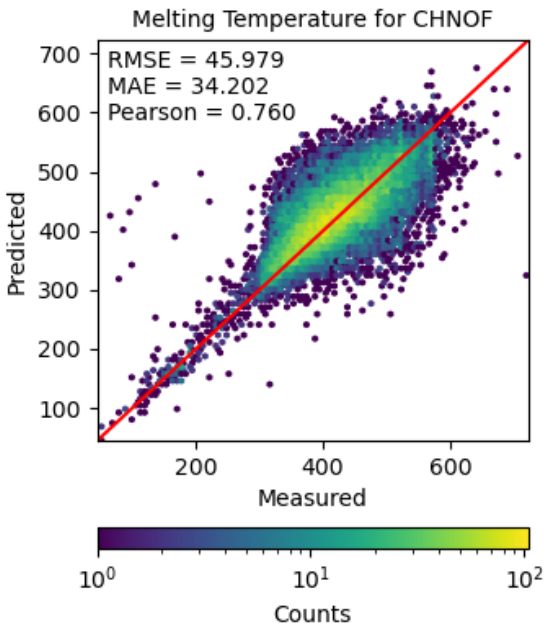

	Num	RMSE	MAE	Pearson
Amino	6228	54.144	40.677	0.628
Amide	8370	46.795	35.871	0.601
Benzyl	24488	46.031	34.369	0.714
CF2+	10994	46.668	34.642	0.744
Furan	612	45.859	35.448	0.726
Imidazole	1981	51.131	38.213	0.594
Indole	1180	50.048	38.538	0.587
Methyl	16251	46.231	34.510	0.734
Naphthalene	590	48.362	38.232	0.646
Nitro	1404	40.998	29.994	0.766
Oxazole	476	43.973	33.372	0.666
Pyrazine	329	47.587	37.842	0.781
Pyrazole	2625	43.455	32.906	0.717
Pyridine	6679	47.052	35.565	0.719
Pyridazine	701	43.372	33.715	0.643
Pyrimidine	2589	49.371	38.287	0.670
Pyrole	1894	50.096	38.438	0.639
Quinazoline	345	48.543	38.385	0.662
Quinoline	2256	48.323	36.739	0.617
1,2,3-Triazole	388	41.985	32.217	0.654
1,2,4-Triazole	860	42.144	32.908	0.710
Total	26813	45.979	34.202	0.760

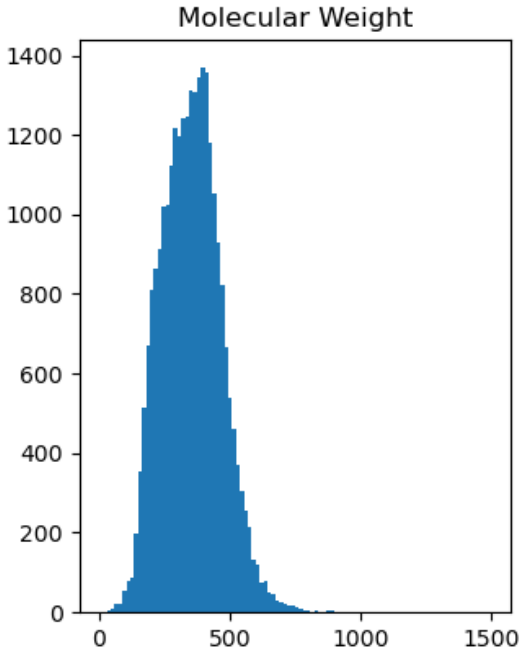

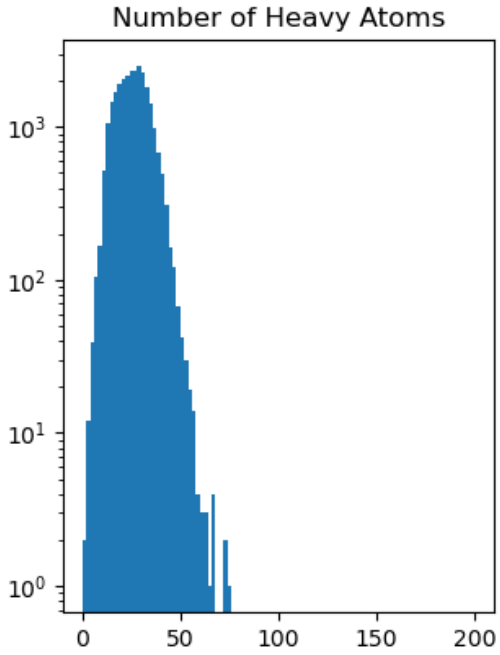

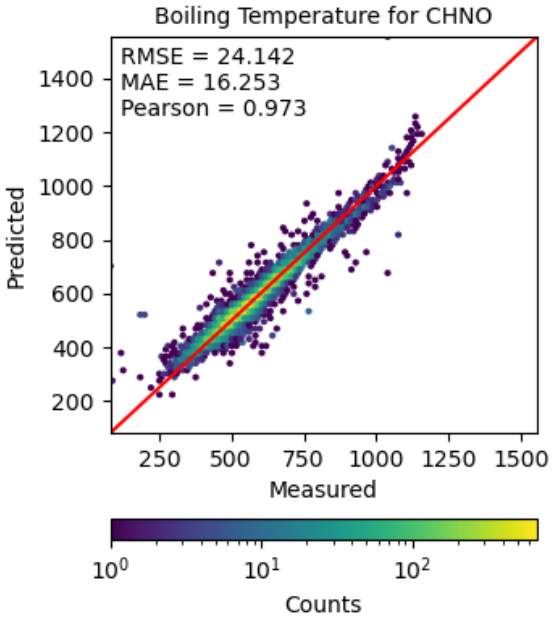

	Num	RMSE	MAE	Pearson
Acridine	98	21.824	16.555	0.954
Amino	3701	22.774	17.206	0.983
Amide	1814	23.724	17.237	0.987
Anthracene	160	18.488	15.260	0.978
Benzyl	9477	22.753	16.719	0.973
Benzofuran	89	21.954	18.391	0.971
Furan	355	24.026	19.364	0.973
Imidazole	353	24.344	14.380	0.966
Indole	314	19.192	12.964	0.988
Methyl	23063	21.661	15.172	0.979
Naphthalene	857	29.776	16.680	0.935
Nitrate	90	44.490	38.695	0.953
Nitro	1186	30.162	18.912	0.948
Pteridine	76	18.633	15.490	0.992
Purine	157	19.340	11.949	0.984
Pyrazine	176	18.608	14.851	0.988
Pyrazole	130	17.349	12.516	0.987
Pyridine	1078	21.593	15.317	0.979
Pyrimidine	423	18.342	13.396	0.991
Pyrole	434	20.983	14.286	0.989
Quinoline	432	20.263	15.557	0.979
Total	29594	24.142	16.253	0.973

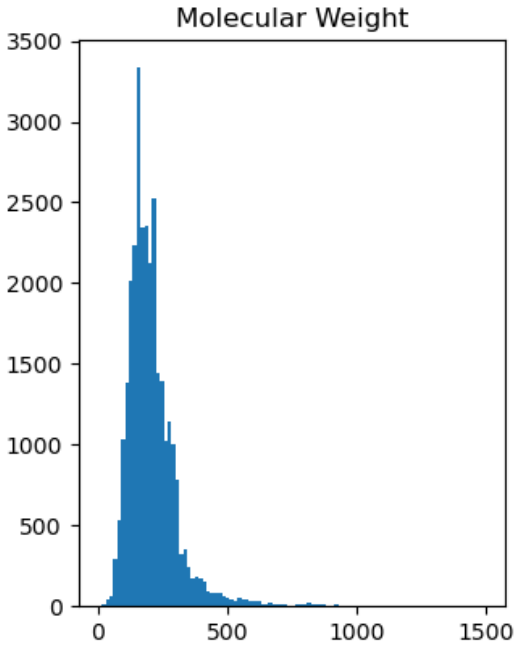

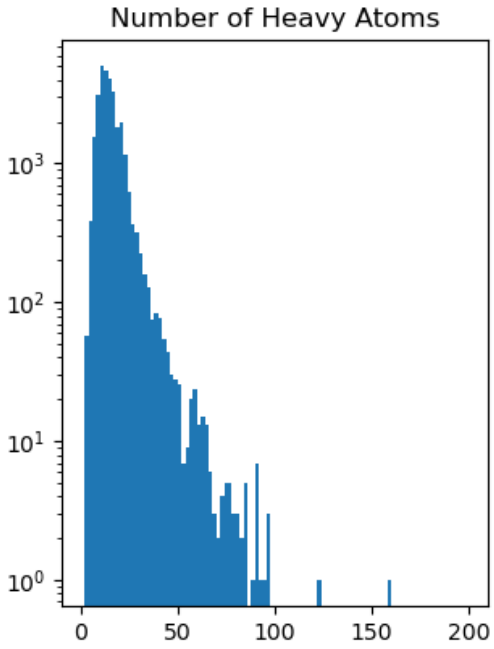

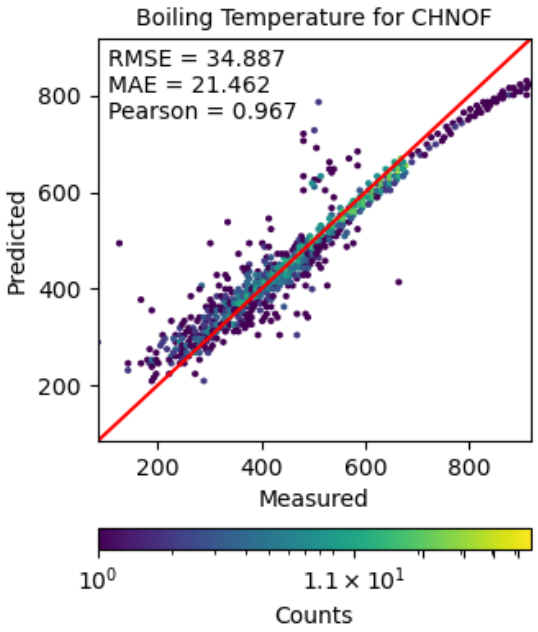

	Num	RMSE	MAE	Pearson
Amino	63	43.651	33.976	0.775
Amide	15	109.162	79.053	0.486
Anthracene	20	113.621	112.898	0.936
Benzyl	405	52.297	34.036	0.681
Benzimidazole	2	227.855	227.855	nan
CF2+	651	38.382	27.535	0.952
Furan	1	21.508	21.508	nan
Imidazole	3	186.456	159.066	1.000
Indole	3	23.912	23.902	0.000
Methyl	1762	25.893	16.188	0.979
Naphthalene	31	109.804	106.796	0.785
Nitrate	3	72.883	67.446	0.983
Nitro	43	45.156	28.406	0.852
Pyrazole	1	80.622	80.622	nan
Pyridine	14	52.276	28.634	0.891
Pyridazine	1	121.728	121.728	nan
Pyrimidine	5	59.528	49.992	0.885
Pyrole	3	23.912	23.902	0.000
1,3,5-Triazine	2	28.039	27.904	1.000
Total	2471	34.887	21.462	0.967

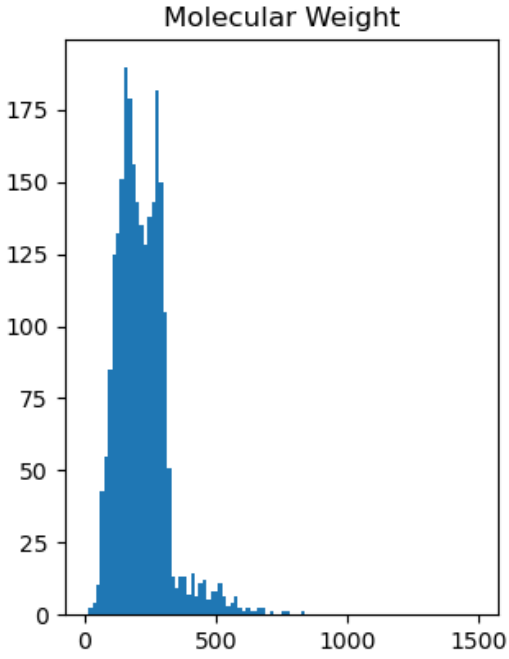

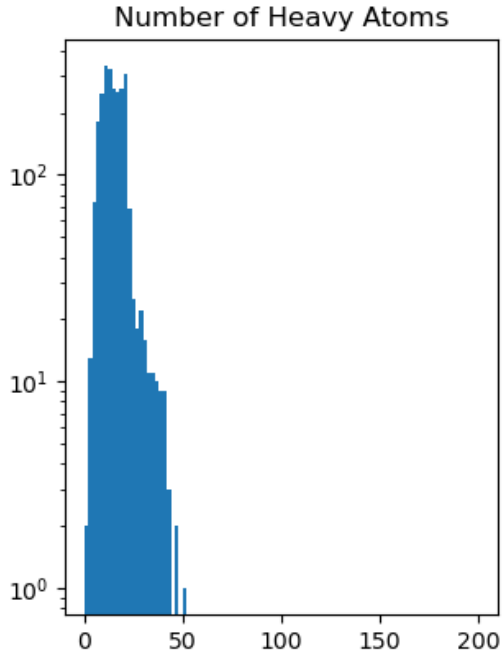

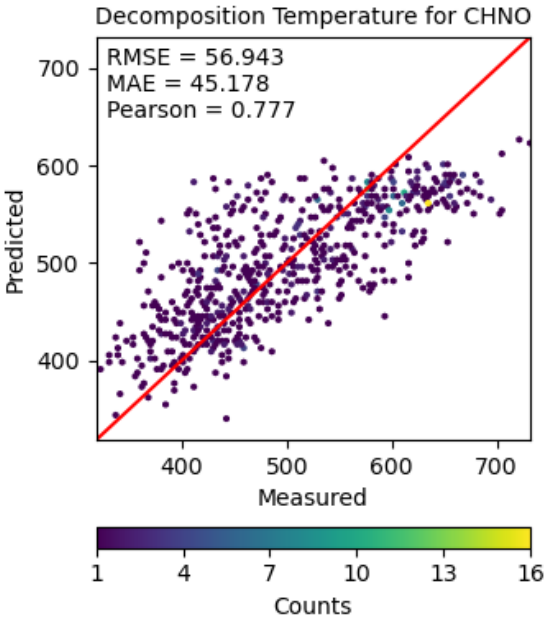

	Num	RMSE	MAE	Pearson
Amino	238	55.323	44.598	0.659
Amide	48	60.512	50.147	0.713
Benzyl	266	67.253	54.794	0.632
Furan	6	44.464	39.925	0.800
Imidazole	3	38.183	34.957	1.000
Methyl	212	57.428	47.102	0.845
Naphthalene	10	112.532	103.269	0.642
Nitrate	12	41.332	35.671	0.418
Nitro	331	56.830	44.609	0.810
Pyrazine	22	56.612	48.576	0.585
Pyrazole	22	45.148	35.335	0.736
Pyridine	30	67.209	53.882	0.426
Pyridazine	5	39.061	31.561	0.959
Pyrimidine	7	32.620	26.321	0.829
Quinoline	4	50.426	44.682	0.591
1,3,5-Triazine	4	54.290	49.307	0.995
1,2,3-Triazole	36	76.104	64.634	0.565
1,2,4-Triazole	72	43.889	34.058	0.765
Total	755	56.943	45.178	0.777

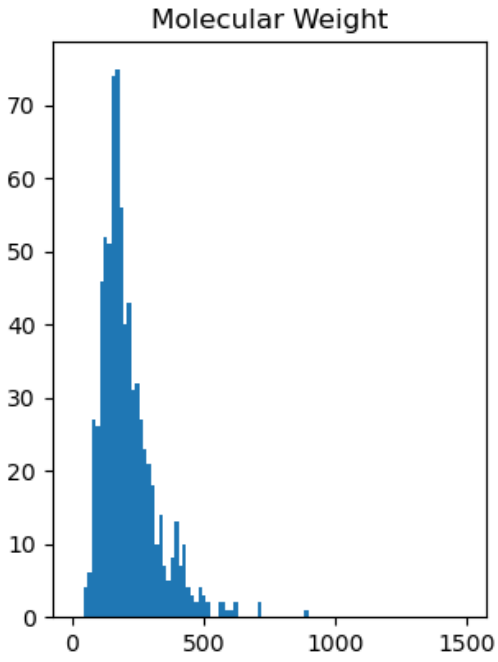

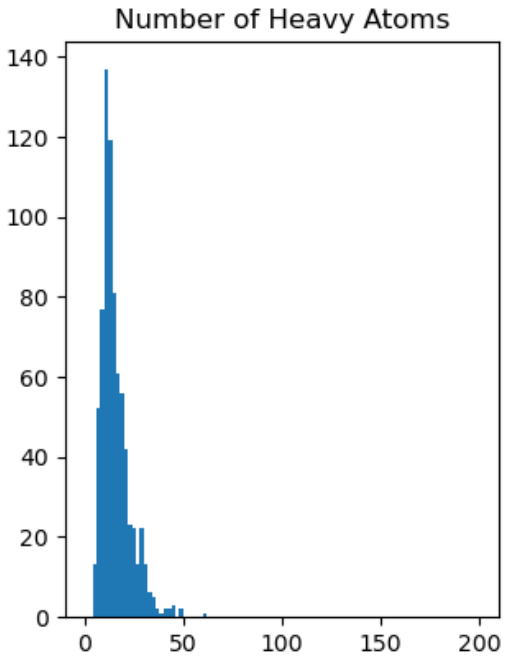

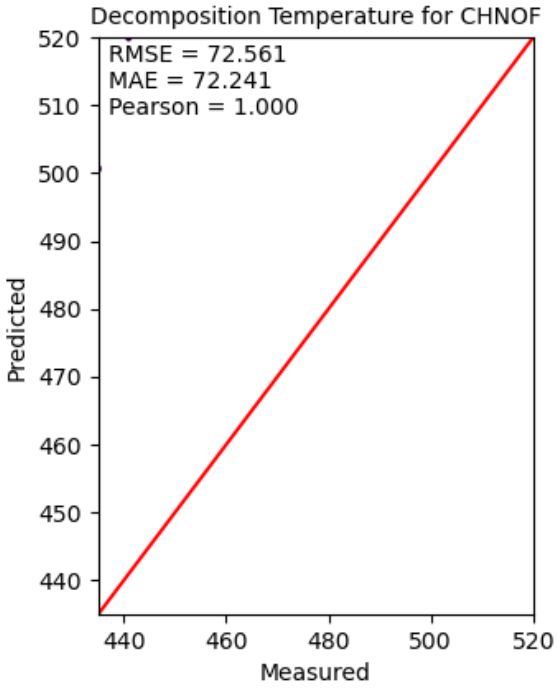

	Num	RMSE	MAE	Pearson
Benzyl	1	79.046	79.046	nan
CF2+	1	65.436	65.436	nan
Methyl	2	72.561	72.241	1.000
1,2,3-Triazole	2	72.561	72.241	1.000
Total	2	72.561	72.241	1.000

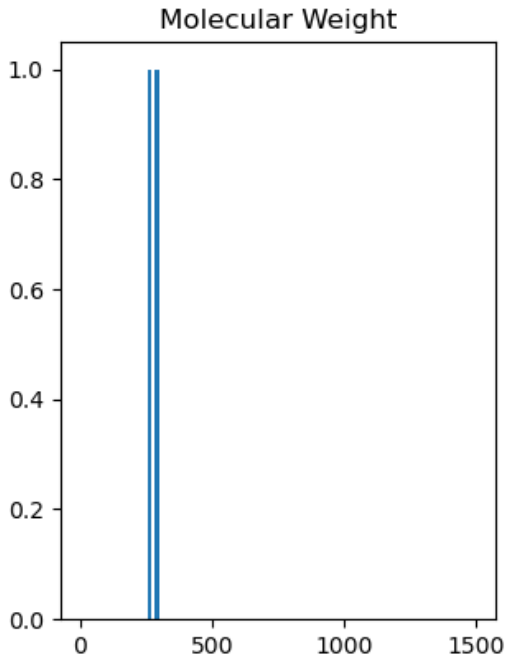

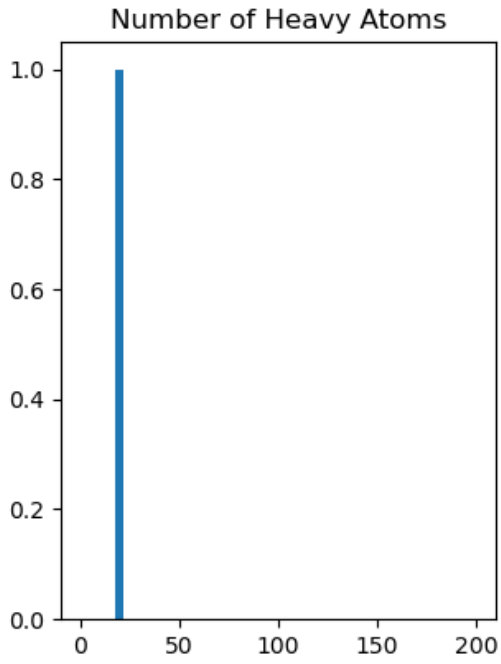

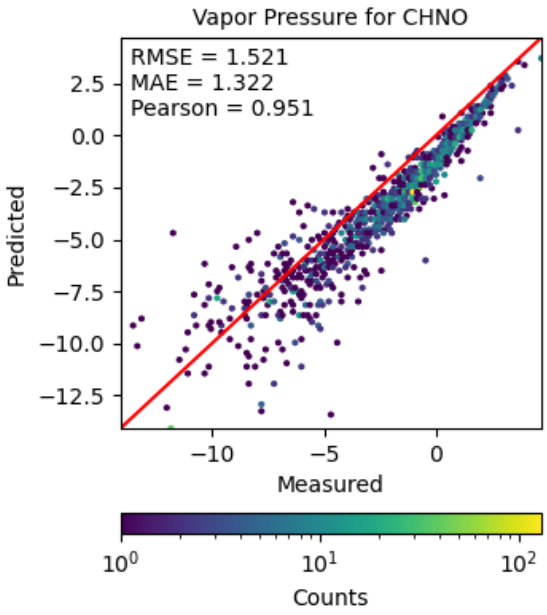

	Num	RMSE	MAE	Pearson
Acridine	4	1.407	1.407	nan
Amino	282	1.587	1.362	0.932
Amide	55	1.619	1.401	0.878
Benzyl	727	1.677	1.448	0.902
Benzofuran	4	1.215	1.183	0.960
Furan	22	1.638	1.466	0.979
Imidazole	7	4.025	3.734	-0.571
Indole	4	1.703	1.459	0.849
Methyl	1780	1.512	1.335	0.951
Naphthalene	34	1.282	1.127	0.952
Nitrate	17	1.179	1.127	0.979
Nitro	101	1.455	1.188	0.936
Purine	4	4.757	4.506	-0.027
Pyrazine	2	1.832	1.831	1.000
Pyrazole	4	3.744	3.506	0.999
Pyridine	70	1.340	1.231	0.946
Pyrimidine	22	2.451	1.799	0.535
Pyrole	8	1.563	1.374	0.864
Quinoline	31	1.275	1.209	0.924
1,3,5-Triazine	9	1.390	1.249	0.815
Total	2417	1.521	1.322	0.951

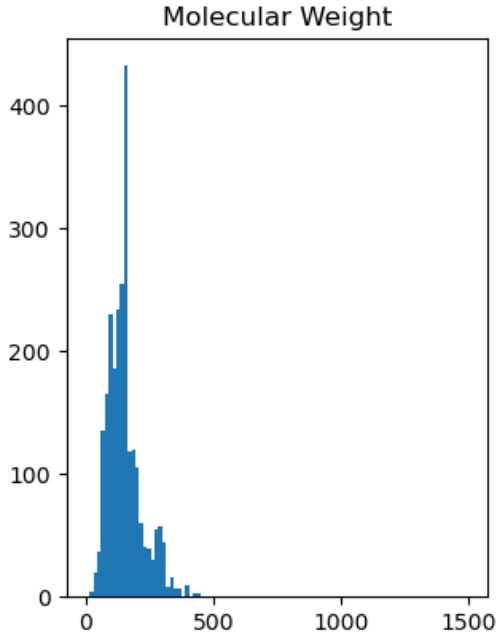

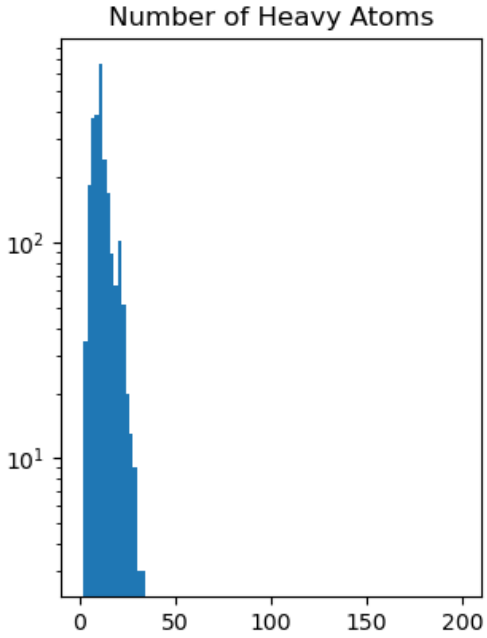

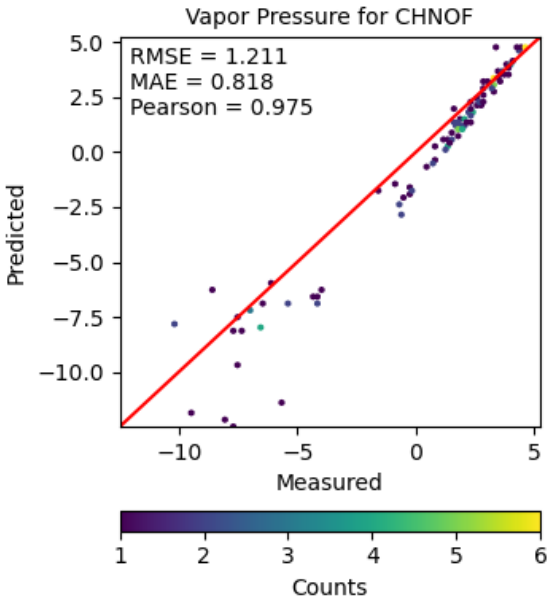

	Num	RMSE	MAE	Pearson
Amino	4	2.620	1.972	0.675
Amide	3	3.626	2.946	-0.828
Benzyl	50	1.818	1.407	0.947
CF2+	99	1.104	0.698	0.986
Methyl	56	1.505	1.146	0.982
Nitro	11	1.838	1.570	0.957
Pyridine	8	1.284	1.089	0.413
Pyrimidine	1	0.525	0.525	nan
Pyrole	1	2.303	2.303	nan
1,2,4-Triazole	2	2.435	2.435	nan
Total	144	1.211	0.818	0.975

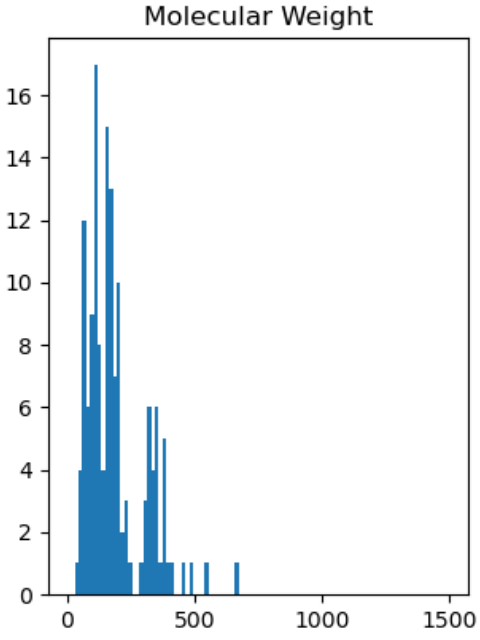

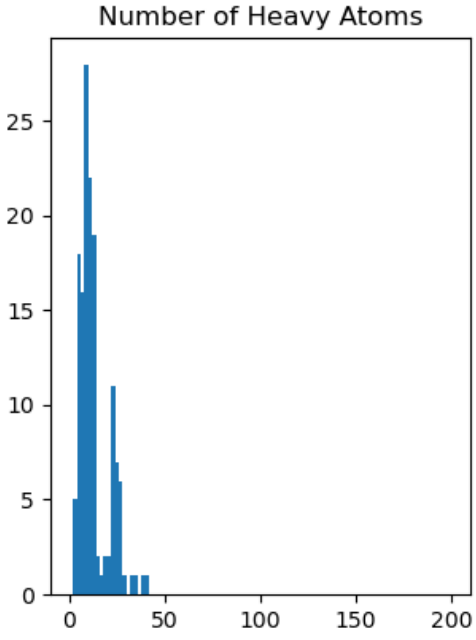

List of Symbols, Abbreviations, and Acronyms

2D	Two-Dimensional
ARL	Army Research Laboratory
CHNO	Carbon, Hydrogen, Nitrogen, and Oxygen
CHNOF	Carbon, Hydrogen, Nitrogen, Oxygen, and Fluorine
CSV	Comma-Separated Value
DEVCOM	U.S. Army Combat Capabilities Development Command
DoD	Department of Defense
EPPI	Energetic Properties Prediction Interface
GUI	Graphical User Interface
H_{50}	Measure of Impact Sensitivity
HoF	Heat of Formation
MAE	Mean Absolute Error
ML	Machine Learning
PETN	Pentaerythritol Tetranitrate
QM	Quantum Mechanical
RA	Robert Appleton
RMSE	Root Mean Square Error
SE	Standard Errors in the Mean
SMILES	Simplified Molecular Input Line Entry System

1 (PDF)	DEFENSE TECHNICAL INFORMATION CTR DTIC OCA
1 (PDF)	DEVCOM ARL FCDD RLB CB TECH LIB